

1 **The effectiveness of solar radiation management for marine cloud brightening**
2 **geoengineering by fine sea spray in worldwide different climatic regions**

3
4 Zhe Song^{1*}, Shaocai Yu^{2*+}, Pengfei Li³⁺, Ningning Yao², Yuhai Sun², Boqiong Jiang², Daniel Rosenfeld⁴

5
6 ¹ Research Center for Air Pollution and Health; Key Laboratory of Environmental Remediation and
7 Ecological Health, Ministry of Education, College of Environment and Resource Sciences, Zhejiang
8 University, Hangzhou, Zhejiang 310058, P.R. China

9 ² School of Environmental Sciences and Engineering, Zhejiang Gongshang University,
10 Hangzhou 310018, China

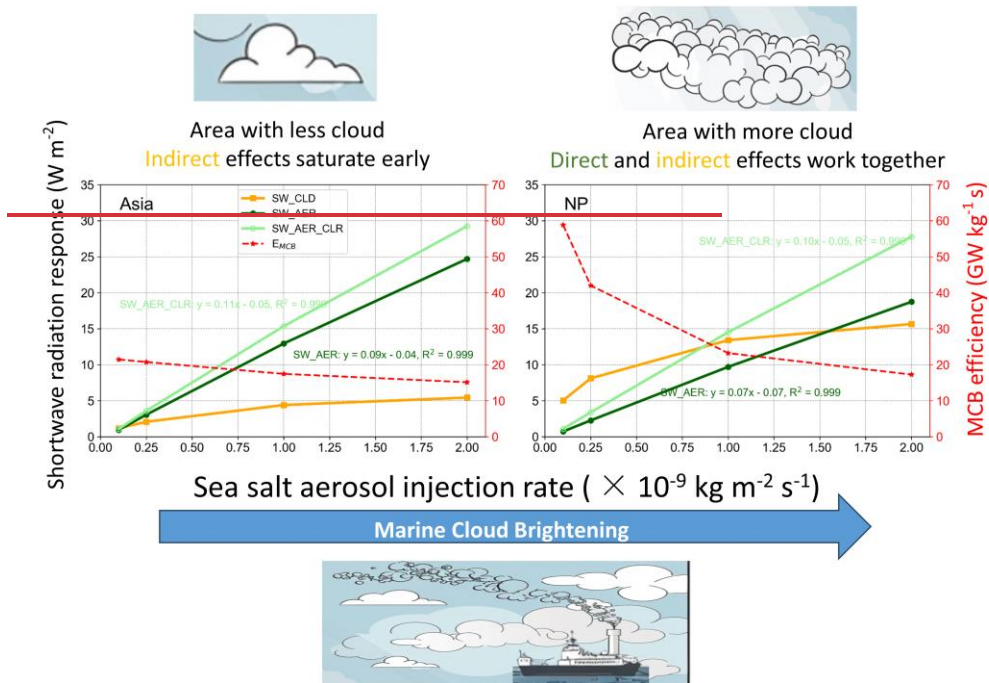
11 ³ State Key Laboratory of Infrared Physics, Shanghai Institute of Technical Physics, Chinese Academy
12 of Sciences, Shanghai 200031, China

13 ⁴ Institute of Earth Sciences, The Hebrew University of Jerusalem, Jerusalem, Israel

14
15
16 *Equal contribution

17 ⁺Correspondence to: Shaocai Yu (shaocaiyu@zjgsu.edu.cn), Pengfei Li (pengfeili@mail.sitp.ac.cn)

18
19 **To be submitted to**
20 **Atmospheric Chemistry and Physics**





Area with less cloud

Indirect effects saturate early

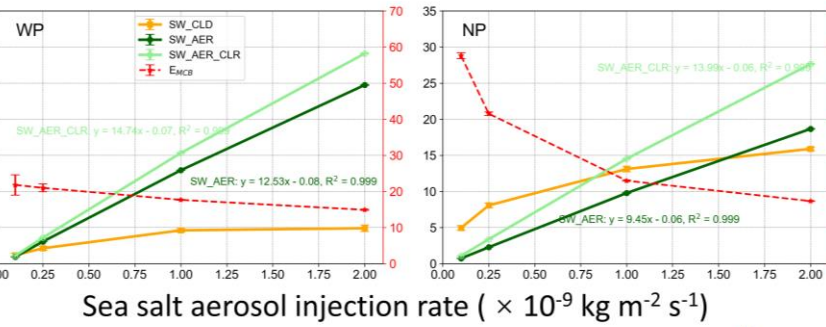


Area with more cloud

Direct and indirect effects work together

Shortwave radiation response ($W m^{-2}$)

MCB efficiency ($GW kg^{-1} s$)



Sea salt aerosol injection rate ($\times 10^{-9} kg m^{-2} s^{-1}$)



23

24

25 **Abstract**

26 Marine Cloud Brightening (MCB) geoengineering aims to inject aerosols over oceans to brighten
27 clouds and reflect more sunlight to offset the impacts of global warming or to achieve localized climate
28 cooling. There is still controversy about the contributions of direct and indirect effects of aerosols in
29 implementing MCB and the lack of quantitative assessments of both. Here, we ~~conducted~~
30 ~~experiments~~designed model simulations with injected sea-salt aerosols in the same framework for five
31 open oceans around the globe. Our results show that a uniform injection strategy that ~~did~~does not depend
32 on wind speed captured the sensitive areas of the regions that produced the largest radiative perturbations
33 during the implementation of MCB. When the injection amounts ~~were~~are low, the sea-salt aerosols
34 ~~dominated~~dominate the shortwave radiation mainly through the indirect effects of brightening clouds,
35 showing obvious spatial heterogeneity. As the indirect ~~effects~~effect of aerosols ~~saturated~~saturates with
36 increasing injection rates, the direct ~~effects still increased~~effect increases linearly and ~~exceeded~~exceeds
37 the indirect effects, producing a consistent increase in the spatial distributions of top-of-atmosphere
38 upward shortwave radiation. ~~Our research emphasizes that MCB was best implemented in areas with~~
39 ~~extensive cloud cover, while the aerosol direct scattering effects remained dominant when clouds were~~
40 ~~scarce~~This study provides quantifiable radiation and cloud variability data for multiple regional MCB
41 implementations and suggests that injection strategies can be optimized by adjusting injection amounts
42 and selecting sensitive areas in the simulations of regional models.

43

44 **Keywords:** marine cloud brightening; solar radiation management; fine sea spray; climatic ocean regions;
45 geoengineering

46

47 1. Introduction

48 As global temperatures continue to rise, the international community is facing an unprecedented challenge
49 to achieve the ambitious goal set in the Paris Agreement of limiting global warming to within 1.5 °C
50 (Mengel et al., 2018). ~~Even the recent~~ One of the key outcomes of the recently concluded 28th Conference
51 of the Parties (COP28) ~~proposing to phase out all fossil fuels from the current energy system to~~
52 ~~achieve~~ was the global goal on adaptation and its framework, it is also reeognized completion of the first
53 Global Stocktake (GST), a mid-term assessment of the progress made by countries toward achieving the
54 climate goals of the Paris Agreement. However, the report highlighted that our current efforts are still
55 insufficient to meet the COP28 goals (<https://www.cop28.com/>); to reduce emissions had fallen short of
56 the intended targets (<https://www.cop28.com/>). Against this backdrop, scientists are turning their
57 ~~attentions~~ attention to more ~~radical and~~ innovative geoengineering methods; by attempting to reduce or
58 offset the impacts of climate change through artificial interventions in the climate (Visoni et al., 2023).
59 Some geoengineering methods seek to capture or remove CO₂ from the atmosphere to increase carbon
60 sinks, while others focus on modifying solar radiation, reducing incoming solar shortwave radiation, or
61 reflecting more sunlight to cool the earth, known as solar radiation management (SRM) (Lenton and
62 Vaughan, 2009). Among these, marine cloud brightening (MCB) has a certain realistic basis and is
63 considered the most likely ~~geoengineering~~ SRM method for regional applications (Latham et al., 2014). It
64 has been observed that exhaust emissions from ocean-going vessels can lead to brighter clouds, with clear
65 ship tracks also visible from satellites, and MCB aims to replicate this effect by spraying sea-salt aerosols
66 (Chen et al., 2012).

67 Aerosol-cloud interactions and their impacts on climate are complex (Rosenfeld et al., 2014, 2019).
68 Injected sea-salt aerosols affect clouds through indirect effects (Paulot et al., 2020). In the case of a
69 constant liquid water content, an increase in cloud droplet number concentration (CDNC) decreases the
70 cloud droplet size, increases the total surface area of cloud droplets, thereby enhancing the cloud albedo,
71 forming brighter clouds, and reflecting more sunlight back to space (the first indirect effect or Twomey
72 effect) (Twomey, 1974). At the same time, the decrease in cloud droplet size suppresses precipitation,
73 thereby increasing the cloud's lifespan and optical thickness (the second indirect effect of aerosols)
74 (Albrecht, 1989). Reducing the cloud drop size induces a faster evaporation and loss of cloud water.
75 However, the effect of the coarse ~~part of the~~ sea spray aerosols has an opposite effect that offsets the loss
76 of liquid water ~~passpath~~ (Liu et al., 2022). In addition, those aerosols that are not injected ~~aerosols into the~~
77 clouds scatter more sunlight back into space through the direct scattering effect (Ahlm et al., 2017;

设置了格式: 字体颜色: 黑色, 英语(美国)

78 Partanen et al., 2012; Zhao et al., 2021). Therefore, this method is also called marine sky brightening
79 (MSB), which can work even when there are no clouds. Here, we collectively refer to the practice of
80 injecting sea-salt aerosols as MCB. ~~MCB has unique advantages compared to other geoengineering
81 schemes. For example, the sprayed aerosols are non-polluting, and can be applied locally to change the
82 regional climate.~~

83 Compared to other geoengineering schemes, such as stratospheric aerosol injection (SAI), MCB has
84 unique advantages. For example, the sprayed aerosols have lower environmental risks and can be applied
85 locally to change the regional climate (Latham et al., 2008). Their deployment costs are relatively low
86 and flexible (Kravitz et al., 2014; Latham et al., 2012, 2014). However, despite these potential advantages,
87 the long-term effects and potential risks of MCB are not fully understood, and there are significant
88 uncertainties as well as ethical, political, and environmental risks. Therefore, most of the current
89 literatures examine the environmental and climate impacts of MCB implementation through modeling.

90 Table S1 ~~summarized~~summarizes the results of current modeling ~~experiments~~simulations on MCB
91 ~~and similar spraying of~~with sea-salt aerosols, as well as their implementation strategies. Most MCB
92 studies ~~used~~use Earth-System Models to assess the impacts of the implementation of MCB on climate.
93 Early MCB studies assumed the effects of MCB implementation by setting a fixed CDNC or directly
94 modifying the cloud effective radius (r_e), ignoring the processes such as generation, transport, dry and
95 wet deposition, and activation of injected sea-salt aerosols, and not including the direct radiative effect of
96 aerosols. With the development of models, researchers started to conduct more detailed studies by
97 injecting aerosols or increasing sea-salt aerosol emissions, taking into account the post-~~treatment~~injection
98 processes of aerosols mentioned above. The implementation region of MCB is crucial, ~~and existing~~
99 research. Existing studies have focused on the impacts of ~~implementing~~ MCB implementation in three
100 key areas: open oceans globally, the equatorial region (between 30°S and 30°N), and coastal areas with
101 widespread marine stratocumulus clouds. ~~Alterskjær et al. (2012)~~Alterskjær et al. (2012) used the cloud-
102 weighted susceptibility function to find the most sensitive regions to the injection of sea-salt aerosols.
103 ~~Similarly, Jones and Haywood (2012)~~Similarly, Jones and Haywood (2012) determined the 10% of the
104 marine regions globally most suitable for implementing MCB through an iterative method. The
105 contributions of direct and indirect effects of aerosols during the implementation of MCB are still
106 controversial and quantitative assessment of both is lacking.

107 Here, we ~~used~~use the two-way coupled Weather Research and Forecasting - Community Multi-scale
108 Air Quality model (WRF-CMAQ-~~model~~), combined with previous studies on the region and injection

109 strategies, to implement MCB in five open oceans worldwide. This study ~~simulated~~simulates the regional
110 radiation and cloud responses caused by injecting sea-salt aerosols. This aims to explore the
111 commonalities and differences in MCB implementation in different regions and to seek the optimal
112 strategy for MCB injection.

114 2. Experiments and methods

115 2.1 Model configuration

116 The two-way coupled ~~Weather Research and Forecasting (WRF v3.4) – Community Multi-scale Air~~
117 ~~Quality (CMAQ v5.0.2) model that considered both direct and indirect effects of aerosols was used in~~
118 ~~this study~~⁴³. ~~In the two-way coupled model, aerosols predicted by CMAQ were~~WRF (v3.4) - CMAQ
119 ~~(v5.0.2) model that considers both direct and indirect effects of aerosols was used in this study (Yu et al.,~~
120 ~~2014). In the two-way coupled model, aerosols predicted by CMAQ are~~ able to affect clouds, radiation,
121 and precipitation simulated by WRF in a consistent online coupled manner (Wong et al., 2012). ~~Yu et al.~~
122 ~~(2014)~~Yu et al. (2014) further extended the two-way coupled WRF-CMAQ model by incorporating the
123 aerosol indirect effects (including the first, second, and glaciation aerosol indirect effects), improving the
124 ability of the WRF-CMAQ model to predict clouds and radiation. ~~Wang et al. (2021)~~Wang et al. (2021)
125 validated this model.

126 The physical schemes of the WRF model are the same as those set in ~~Yu et al. (2014)~~Yu et al. (2014),
127 including the asymmetric convective model (ACM2) for a planetary boundary layer (PBL) scheme (Pleim,
128 2007), the Morrison 2-moment cloud microphysics scheme (~~Morrison et al., 2009~~)(Morrison et al., 2009),
129 the Kain-Fritsch (KF2) cumulus cloud parameterization, the Rapid Radiative Transfer Model for General
130 Circulation Models (RRTMG) longwave and shortwave radiation schemes, and the Pleim-Xiu (PX) land-
131 surface scheme. The meteorological initial and boundary conditions were provided by the National Center
132 for Environmental Prediction (NCEP) final analysis dataset (FNL) with a spatial resolution of $1^{\circ} \times 1^{\circ}$ and
133 temporal resolution of 6 h. The carbon bond gas-phase chemical mechanism (CB05) and aerosol module
134 of AERO6 were used in the CMAQ model. The anthropogenic emissions were taken from the
135 Hemispheric Transport of Air Pollution (HTAP_V2) projects (Janssens-Maenhout et al., 2015). The
136 biogenic emissions were estimated by the Biogenic Emissions Inventory System version 3.14 (BEISv3.14)
137 model (Carlton and Baker, 2011). Sea salt emissions were calculated online in CMAQ and were divided
138 into open-ocean and surf-zone emissions. ~~In the open ocean, Gong (2003)~~In the open ocean, Gong (2003)
139 extended the sea-salt aerosol parameterization of ~~Monahan et al. (1986)~~Monahan et al. (1986) to

140 submicron sizes, with the emission flux being linearly proportional to the ocean area covered by whitecaps,
141 ~~The geometric mean diameter of accumulation mode sea-salt aerosols in the CMAQ ranged from 0.2651~~
142 ~~to 0.8187 μm . The particle size distributions of the emitted sea-salt aerosols were~~CMAQ represents the
143 ~~atmospheric particle distribution as the superposition of three log-normal modes, the Aitken,~~
144 ~~Accumulation, and Coarse modes (Binkowski and Roselle, 2003). The particle size distribution and the~~
145 ~~geometric standard deviation of the emitted sea-salt aerosols are~~ adjusted to the local relative humidity
146 before mixing with the ambient particle modes (Zhang et al., 2005). ~~Surf zone emissions were calculated~~
147 ~~using the open ocean source function of Gong (2003)~~The geometric mean diameter of accumulation mode
148 ~~sea-salt aerosols in the CMAQ ranged from 0.2651 to 0.8187 μm , with the geometric standard deviation~~
149 ~~constrained between 1.76 and 1.83. Surf-zone emissions were calculated using the open ocean-source~~
150 ~~function of Gong (2003), with a fixed whitecap coverage of 100% and a surf-zone width of 50 m. Kelly~~
151 ~~et al. (2010)~~Kelly et al. (2010) provided a detailed description of these processes. In the CMAQ model,
152 the number concentration emission rate was calculated from the mass emissions rate as follows:

$$E_{3n} = \left(\frac{6}{\pi}\right) \left(\frac{E_n}{\rho_n}\right) \quad (1)$$

$$E_0 = \frac{\sum_n E_{3n}}{D_{gv}^3 \exp\left(-\frac{9}{2} \ln^2 \sigma_g\right)} \quad (2)$$

155 where E_n was the mass emissions rate for species n and ρ_n was the density for that species. The sum
156 $\sum_n E_{3n}$ was taken over all emitted species. The geometric mean diameter for mass or volume, D_{gv} , was
157 given by $D_{gv} = D_g \exp(3 \ln^2 \sigma_g)$ from the Hatch-Choate relations for a lognormal distribution (Binkowski
158 and Roselle, 2003). This study used Geographic Information System software (ArcGIS) to obtain the
159 open-ocean and surf-zone fractions for each grid within the modeling domain from shoreline information.
160 The modeling domains of the five regions were almost entirely open ocean, with surf-zone fractions of
161 less than 0.01%.

162 2.2 Experimental setup

163 As summarized in Table S1, the MCB geoengineering implementation areas included the globe, the
164 equator (30°S–30°N), regions with extensive coverages of marine stratocumulus clouds, and so on.
165 Therefore, based on previous experimental designs, we ~~used~~use the WRF-CMAQ model to simulate the
166 injections of sea-salt aerosols in the five open ocean regions (Fig. 1c). These regions ~~were Asia~~are WP
167 ~~and NP~~, located in ~~East Asia on~~the western ~~side of the~~and northern Pacific Ocean; Equa, ~~situated~~located
168 in the Philippine Sea along the equator; and NP, SP, and SA, ~~which referred to~~located in the ~~North~~south

设置了格式: 字体: +西文正文 (等线), 五号

设置了格式: 字体: +西文正文 (等线), 五号

169 Pacific, ~~South Pacific~~, and ~~Southsouth~~ Atlantic, respectively. ~~These~~The three regions, NP, SP and SA, are
170 located along the western coast of continents, were considered to have extensive coverage of marine
171 stratocumulus clouds and were the most suitable areas for implementing MCB (Alterskjær et al., 2012;
172 Hill and Ming, 2012; Jones et al., 2009; Partanen et al., 2012; Stuart et al., 2013).

173 The grid numbers of WRF and CMAQ ~~were~~are 190×190 and 173×173, respectively, and both
174 ~~had~~have a horizontal resolution of 12 km, with 29 vertical layers from the surface to about 21 km altitude.
175 The simulation period for the ~~Asia~~WP, Equa, and NP regions in the northern hemisphere ~~was~~is from July
176 24, 2018, to September 1, 2018, while for the SP and SA regions in the southern hemisphere, the
177 simulation period ~~was~~is from February 24, 2023, to April 1, 2023. The first 8 days of the model
178 simulations ~~were~~are considered as the spin-up period to minimize the impacts of initial chemical
179 conditions.

180 The results of the Base simulations with the model settings described above and default sea salt
181 emissions (no aerosol injection) were obtained. As can be seen, there are significant differences in the
182 cloud distributions for the five ocean regions in the Base simulations during the study period, with wider
183 distributions of liquid clouds in the NP, SP, and SA regions, but fewer clouds in the WP and Equa regions
184 (Fig. 2, first column). Cloud heights are distributed between 500–2000 m, centered at 1000 m (Fig. S1,
185 first column). The cloud fraction, CDNC, liquid water path (LWP), and sea-salt aerosol concentrations in
186 the Base simulations for each region are summarized in Table 1.

187 We ~~tested~~est four different sea-salt aerosol injection ~~methods~~strategies, wind-speed-dependent
188 ~~Natural~~×5, ~~Wind-adjusted~~, ~~Fixed-wind-adjusted at 10⁻⁹ kg m⁻² s⁻¹~~ and ~~Fixed-wind-adjusted-uniform~~
189 ~~injections of sea salt aerosols at a fixed rate of 10⁻⁹ kg m⁻² s⁻¹~~. All additional injected sea-salt aerosols
190 ~~were~~are in the accumulation mode. In this study, the geometrical mean dry diameter of sea-salt aerosols
191 injected into the five regions ~~was~~is about 0.11–0.15 μm, and ~~was~~is similar for all emission scenarios.

192 ~~Natural~~×5: ~~Increased~~Increase the emission rates of accumulation mode sea-salt aerosols by a factor
193 of 5 (Hill and Ming, 2012). This ~~was~~is a simple wind-speed-dependent increase. The injection rates in the
194 five regions ~~were~~are equivalent to 0.03031–0.09085×10⁻⁹ kg m⁻² s⁻¹ (Table S2).

195 ~~Wind-adjusted~~: Salter et al. (2008) designed a spray vessel for injecting sea-salt aerosols with a
196 ~~spray efficiency that was dependent on wind speed and was expected to achieve maximum spray outputs~~
197 ~~at wind speeds between 6–8 m s⁻¹. The threshold wind speed was set to 7 m s⁻¹ and the spray efficiency~~
198 ~~at lower wind speeds was 1.5 times the wind speed. We used the source function of Partanen et al. (2012)~~
199 ~~as follows, where u was the 10 m wind speed. For example, at wind of 7 m s⁻¹ the injection rate would be~~

带格式的: 缩进: 首行缩进: 2 字符

设置了格式: 字体: 非加粗

200 $0.26 \times 10^{-9} \text{ kg m}^{-2} \text{ s}^{-1}$.

201 **Wind-adjusted:** Salter et al. (2008) designed a spray vessel for injecting sea-salt aerosols with a
202 spray efficiency that was dependent on wind speed and was expected to achieve maximum spray outputs
203 at wind speeds between 6–8 m s⁻¹. The threshold wind speed was set to 7 m s⁻¹ and the spray efficiency
204 at lower wind speeds raised to the power of 1.5. We use the source function of Partanen et al. (2012) as
205 follows, where u is the 10 m wind speed. For example, at wind of 7 m s⁻¹ the injection rate will be $0.26 \times$
206 $10^{-9} \text{ kg m}^{-2} \text{ s}^{-1}$.

$$207 F_{m, \text{baseline}} = \begin{cases} 5 \times 2.8 \times 10^{-12} \times \left(\frac{u}{1 \text{ m s}^{-1}}\right)^{1.5} \text{ kg m}^{-2} \text{ s}^{-1}, & u < 7 \text{ m s}^{-1} \\ 5 \times 2.8 \times 10^{-12} \times 7^{1.5} \text{ kg m}^{-2} \text{ s}^{-1}, & u \geq 7 \text{ m s}^{-1} \end{cases} \quad (3)$$

208 **Fixed at $10^{-9} \text{ kg m}^{-2} \text{ s}^{-1}$:** Unlike the previous two injection methods, the injections of sea-salt aerosols
209 at a fixed rate of $10^{-9} \text{ kg m}^{-2} \text{ s}^{-1}$ were not dependent on wind speed and increased uniformly over all
210 ocean grids. Injecting sea-salt aerosols at a fixed rate identified the geographic areas that were most
211 sensitive to increased sea-salt aerosols and produced the largest top-of-atmosphere (TOA) radiative
212 perturbations (Alterskjær et al., 2012). Many other studies have used this method (Goddard et al., 2022;
213 Horowitz et al., 2020; Mahfouz et al., 2023). Uniform injections of sea-salt aerosols throughout the region
214 ignored aerosol transports and dispersion at the boundary. Therefore, based on the results of a fixed 10^{-9}
215 $\text{kg m}^{-2} \text{ s}^{-1}$ injection rate, we identified the geographical regions (30×50 grid points, approximately 360
216 $\text{km} \times 600 \text{ km}$, away from the domain boundary) in five ocean areas where the TOA radiative perturbations
217 caused by uniform injection were the largest, and the most sensitive. Table S3 shows the locations of these
218 sensitive regions. The injection amount in the sensitive region at a fixed $10^{-9} \text{ kg m}^{-2} \text{ s}^{-1}$ injection rate is
219 found to be about 1/20 of those in the full domain.

设置了格式: 字体: Times New Roman, 字体颜色: 红色

220 **Fixed-wind-adjusted:** To rule out differences in radiative and cloud response due to wind
221 variabilities on spray rates, we performed an additional adjustment. Similar to **Natural×5**, the
222 injections of sea-salt aerosols were also dependent on the wind speed but the integrated amounts in the
223 region were set to be equal to the case that all area had a fixed rate of $10^{-9} \text{ kg m}^{-2} \text{ s}^{-1}$ (**Fixed**).

设置了格式: 字体: Times New Roman, 小四

224 2.3 Calculations

225 ~~The calculation method related to radiation, cloud properties, and cloud radiation forcing was based on~~
226 ~~Goddard et al. (2022), briefly described here as follows. This study focused on the shortwave radiative~~
227 ~~flux responses at the TOA due to the injections of sea salt aerosols, which was consistent with the~~
228 ~~definition of effective radiation forcing (ERF) (Forster et al., 2007). The sea surface temperature in the~~

229 ~~model was preset by NCEP-FNL, so the model's surface temperature and upward longwave radiation~~
230 ~~would not respond to the increased sea-salt aerosols. The total upward shortwave radiation flux (SW_TOT)~~
231 ~~at the TOA was under the all-sky conditions. The responses of SW_TOT to the injections of sea salt~~
232 ~~aerosols could be divided into the cloud radiation effects (SW_CLD, excluding the influence of aerosols)~~
233 ~~and the direct scattering effects when clouds were present (SW_AER).~~

234 The calculation method related to radiation, cloud properties, and cloud radiation forcing is based on
235 Goddard et al. (2022), briefly described here as follows. This study focuses on the shortwave radiative
236 flux responses at the TOA due to the injections of sea-salt aerosols, which is consistent with the definition
237 of effective radiation forcing (ERF) (Forster et al., 2007). The sea surface temperature in the model is
238 preset by NCEP-FNL, so the model's surface temperature and upward longwave radiation would not
239 respond to the increased sea-salt aerosols. The total upward shortwave radiation flux (SW_TOT) at the
240 TOA is under the all-sky conditions. The responses of SW_TOT to the injections of sea-salt aerosols
241 could be divided into the cloud radiation effects (SW_CLD, excluding the direct effect of the aerosols)
242 and direct scattering effects when clouds are present (SW_AER).

$$243 \quad \text{SW_TOT} = \text{SW_CLD} + \text{SW_AER} \quad (4)$$

244 The diagnosis of CLEAN-SKY (no aerosols) ~~was~~ not considered in the previous WRF-CMAQ
245 model. So in this study, we ~~extended~~ extend this feature in the WRF-CMAQ model using the methodology
246 of ~~Ghan et al. (2012)~~ Ghan et al. (2012) by performing a double radiative call at each time step to calculate
247 radiation variables related to CLEAN-SKY (SW_CLD). We ~~have~~ also ~~studied~~ study the impacts of
248 injecting sea-salt aerosols on the upward shortwave radiation flux at the TOA under the clear-sky
249 conditions (SW_AER_CLR). At this time, only the direct scattering effect of aerosols existed, which
250 ~~was~~ considered to be the maximum MSB potential generated by injecting sea-salt aerosols when there
251 ~~were~~ is no clouds. ~~Unless otherwise specified, all results in this study were monthly averages.~~ cloud.

252 Due to the different amounts of sea-salt aerosols injected in different ways, it ~~resulted~~ results in
253 different SW_TOT responses. Therefore, we ~~proposed~~ propose the concept of MCB efficiency (E_{MCB}) to
254 measure the relationships between the amount of sea-salt aerosol injections and the resulting radiation
255 flux responses. (Table S2).

$$256 \quad E_{MCB} = \frac{\text{SW_TOT response due to injection of sea-salt aerosol (W m}^{-2}\text{)}}{\text{Sea-salt aerosol injections (kg m}^{-2}\text{ s}^{-1}\text{)}} \quad (5)$$

257 ~~It measured~~ This is a measure of the mass efficiency of MCB implementing MCB in different regions,
258 that ~~was~~ is, how much SW_TOT responses ~~were~~ are expected to be generated by injecting sea-salt aerosols

带格式的: 缩进: 首行缩进: 0.74 厘米

at a rate of $1 \text{ kg m}^{-2} \text{ s}^{-1}$. $E_{\text{MCB}} = 1$ means that injecting 1 kg of sea-salt aerosols per unit time in the current study area ~~wasis~~ expected to produce a 1 GW (10^9 W) SW_TOT response. Note that this value (E_{MCB}) ~~wasis~~ based on model calculations under specific atmospheric conditions within the study region and ~~wasis~~ only used to analyze the sensitivities of the radiative flux to different injection methods and injection amounts.

This study ~~foeused~~~~focuses~~ on the changes in liquid clouds and evaluated the responses in cloud condensation nuclei (CCN), cloud fraction, CDNC, r_e , ~~liquid water path (LWP)~~, cloud optical thickness (COT), and cloud albedo due to the injections of sea-salt aerosols. These calculations ~~were~~~~are~~ shown in Supplementary Text S1.

Cloud radiation forcing (CRF) parameters can be used to quantify the responses of SW_CLD to changes in cloud cover or cloud albedo, defined as follows (Goddard et al., 2022):

$$\text{CRF}_{\text{param}} = \alpha_c f \quad (6)$$

where α_c ~~wasis~~ mean cloud albedo and f ~~wasis~~ mean cloud fraction.

The CRF parameters ~~could~~~~can~~ be approximated using the perturbation method as follows (Goddard et al., 2022):

$$\text{CRF}'_{\text{param}} = \alpha'_c \bar{f} + \bar{\alpha}_c f' + \alpha'_c f' \quad (7)$$

where the first term on the right-hand side ~~indicated~~~~indicates~~ the changes in $\text{CRF}_{\text{param}}$ driven by the perturbation of cloud albedo, the second term ~~indicated~~~~indicates~~ the changes driven by the perturbation of cloud fraction, and the third term ~~denoted~~~~denotes~~ the changes driven by the interactions of the two. The horizontal bars on α_c and f ~~were~~~~are~~ defined as the monthly means of the Base, and the prime (') ~~defined~~~~defines~~ the monthly mean differences between the sensitivity experiments and Base. The fourth column of Fig. ~~S24S23~~ shows that the differences between $\text{CRF}_{\text{param}}$ and $\text{CRF}'_{\text{param}}$ ~~were~~~~are~~ small enough that the perturbation method ~~could~~~~can~~ be used to approximate the $\text{CRF}'_{\text{param}}$.

~~The changes in cloud albedo were driven by multiple processes. Based on Quaas et al. (2008) and Christensen et al. (2020), Goddard et al. (2022) established the following equation to assess the relative effects of CDNC, LWP, and mean cloud fraction on the responses of SW_CLD due to the injections of sea salt aerosols:~~

$$\frac{\Delta \alpha}{\Delta \ln \text{AOD}} = f \Delta \alpha_e (1 - \alpha_e) \left(\frac{1}{3} \frac{\Delta \ln \text{CDNC}}{\Delta \ln \text{AOD}} + \frac{5}{6} \frac{\Delta \ln \text{CLWP}}{\Delta \ln \text{AOD}} + \frac{\Delta \ln f}{\Delta \ln \text{AOD}} \right) \quad (8)$$

~~The changes in cloud albedo are driven by multiple processes. Based on Quaas et al. (2008) and Christensen et al. (2020), Goddard et al. (2022) established the following equation to assess the relative~~

289 effects of CDNC, LWP, and mean cloud fraction on the responses of SW_CLD due to the injections of
290 sea-salt aerosols:

$$\frac{\Delta\alpha}{\Delta\ln\text{AOD}} = f\Delta\alpha_c(1 - \alpha_c) \left(\frac{1}{3} \frac{\Delta\ln\text{CDNC}}{\Delta\ln\text{AOD}} + \frac{5}{6} \frac{\Delta\ln\text{CLWP}}{\Delta\ln\text{AOD}} + \frac{\Delta\ln f}{\Delta\ln\text{AOD}} \right) \quad (8)$$

292 where α ~~was~~ is the planetary albedo, Δ ~~represented~~ represents the difference in monthly average results
293 between sensitivity experiments and Base simulations, and α_c ~~was~~ is the cloud albedo. The three terms
294 inside the right parenthesis ~~represented~~ represent the relative contributions of Twomey effect, LWP effect,
295 and cloud fraction effect, respectively, with the latter two related to the second aerosol indirect effect
296 (Albrecht, 1989).

297 The perturbations by generating three ensemble members for each experiment in each region were
298 added. The results of all sensitivity experiments are compared to those of Base simulations. Unless
299 otherwise specified, all results in this study are shown as overall regional monthly averages of the
300 ensemble.

302 3. Results

303 3.1 The impacts of different injection strategies on shortwave radiation at the TOA.

304 In modeling studies, ~~using different variations in~~ using methods used to increase sea-salt aerosols may lead to
305 different conclusions, and ~~this discrepancy-these variations~~ may be one of the reasons for differences in
306 the assessments of MCB potentials in the previous studies. In this study, sea-salt aerosols injected in
307 different strategies (with dry diameters of about 0.11–0.15 μm , Fig. 1a) ~~increased~~ increase the SW_TOT
308 at the TOA by ~~0.06–24.5007–25~~ 0.06–24.5011–25 W m^{-2} in the five ocean regions (Fig. 23a). The Natural \times 5 and Wind-
309 adjusted ~~methods~~ strategies, which ~~rely~~ rely on wind speeds, ~~injected~~ inject sea-salt aerosols of ~~0.03031–~~
310 ~~0.09085~~ 0.03031– and ~~0.18–0.21~~ 0.18–0.21 $\times 10^{-9} \text{ kg m}^{-2} \text{ s}^{-1}$ into the five regions, respectively, ~~resulting and result~~ result
311 variations of ~~0.0607–2.08 and 1.35 and 1.4–8.474~~ 0.0607–2.08 and 1.35 and 1.4–8.474 W m^{-2} (Table S2), respectively. ~~Except for the Equa~~
312 ~~region, the other four regions can initially achieve the radiation flux responses required to offset the~~
313 ~~radiative forcing of 3.7 W m⁻² due to doubling of atmospheric CO₂ concentration since industrialization~~
314 ~~(Latham et al., 2008; Ramaswamy et al., 2001). (Fig. 3a and Table 2).~~ Uniformly injections of sea-salt
315 aerosols at a fixed rate of $10^{-9} \text{ kg m}^{-2} \text{ s}^{-1}$ ~~resulted~~ result in SW_TOT changes of ~~10.96–24.5011–25~~ 10.96–24.5011–25 W m^{-2}
316 in the five regions. ~~This value far exceeded the radiation flux response envisioned for offsetting~~
317 ~~geoengineering, so we only used it to explore the sensitivities of different injection methods and regional~~
318 ~~responses, and subsequent studies on the impacts of injecting sea salt aerosols in sensitive areas on the~~

entire region. The three continental west coast stratocumulus regions of NP, SP, and SA had have the most significant SW_TOT responses, all exceeding 20 W m^{-2} , while the SW_TOT responses in the AsiaWP and Equa regions are 18 and Equa regions were 17.34 and 10.96 11 W m^{-2} , respectively.

Injecting the same amount of sea-salt aerosols resulted results in substantial variations in SW_TOT responses across the different regions (Fig. S1S2). The sea-salt aerosols sprayed in the Fixed-wind-adjusted experiments were are also dependent on wind speed, but the amount of emission rate integrated in the full domain was is consistent with the fixed rate of $10^{-9} \text{ kg m}^{-2} \text{ s}^{-1}$, ruling out the differences caused by the amount of injected sea-salt aerosols. Although both methods injected strategies inject the same amounts of sea-salt aerosols, the SW_TOT responses they produced were produce are significantly different. The Fixed-wind-adjusted method resulted strategy results in SW_TOT changes of 5.00–19.780–20 W m^{-2} in the five regions; (Fig. 3a), indicating that the shortwave radiation flux changes caused by wind-speed-dependent injections were are smaller than those caused by uniformly injections, and showed regional differences. Due to the different amounts of sea salt aerosol injected in different ways, it resulted in different SW_TOT responses. Therefore, we proposed the concept of MCB efficiency (E_{MCB}) to measure the relationships between the amounts of sea salt aerosol injections and the resulting radiation flux responses. $E_{\text{MCB}} = 1 \text{ GW kg}^{-1} \text{ s}$ means that injecting 1 kg of sea salt aerosols per unit time in the current study area was expected to produce a 1 GW (10^9 W) SW_TOT response.

Figure 3b shows the E_{MCB} values of different sea-salt injection strategies in the five regions. Overall, MCB implementation was is more efficient in the NP, SP, and SA regions, while it was is less efficient in the AsiaWP and Equa, which was is similar to the previous SW_TOT response results. E_{MCB} also varied varies for different injection methods strategies. In the NP, SP, and SA regions, the E_{MCB} values of the Natural $\times 5$ and Wind-adjusted methods strategies with relatively small injection amounts were are higher. With the increases in sea salt aerosols injections, E_{MCB} decreased (discussed below), than the other two strategies with large injection amounts. At the same injection amount, injecting at a fixed rate shows higher E_{MCB} compared relative to injections dependent depending on wind speed, as consistently shown in all five regions; (Fig. 3b). Since the number flux of aerosols increased with the decreases of the injected aerosol particle size for the same mass flux, we examined the MCB efficiency in units of aerosol number concentration (Fig. S3). The results show that the number efficiency of MCB is proportional to the injection rate of aerosol number (Fig. S3c). In the same quality injected, the aerosol number varies greatly (Fig. S3d).

The productions of sea-salt aerosols in nature were are strongly correlated with wind speed, and most

设置了格式: 字体: 非加粗

350 models associated sea-salt aerosol emissions with wind speed (Ahlm et al., 2017; Grythe et al., 2014).
351 Injection strategies depending on wind speed ~~made~~ make the distributions of added sea-salt aerosols closer
352 to the natural distributions. In natural environments, sea-salt aerosol emissions in strong-wind areas (e.g.,
353 storm or typhoon areas) and surf zones are usually much larger than in weak-wind areas. Therefore,
354 injection ~~methods~~ strategies depending on wind speed ~~concentrated~~ concentrate the added sea-salt aerosols
355 in strong-wind areas and surf zones, while the weak-wind regions ~~increased~~ increase relatively little sea-
356 salt aerosols (Fig. S2S4). Injecting uniformly at a fixed rate in the model ~~would~~ will result in a large
357 increase of sea-salt aerosols in places with originally low aerosol concentrations (e.g., weak-wind regions).
358 Therefore, when using models to simulate the injections of sea-salt aerosols by increasing the emission
359 rate, it ~~was~~ is necessary to consider the impacts of different injection methods on the distributions of sea-
360 salt emissions. Using a uniformly increasing method independent of wind speed can not only avoid the
361 situation of a smaller increase in sea-salt emissions in regions with lower wind speeds, but can also
362 identify the geographical areas most sensitive to the increased sea-salt aerosols and producing the largest
363 TOA radiation perturbations (Alterskjær et al., 2012).

364 ~~Uniform injections of sea salt aerosols throughout the region ignored the transport and diffusion of~~
365 ~~aerosols. Therefore, we captured the geographical areas with the most sensitive and largest TOA radiation~~
366 ~~disturbances due to uniform injections in various ocean regions (30 × 50 grids, approximately 360 km ×~~
367 ~~600 km, and away from the domain boundaries).~~ Injecting sea-salt aerosols in the sensitive areas with the
368 same uniform injections (10^{-9} kg m⁻² s⁻¹, the injection rate is about 1/20 of the full domain injection)
369 ~~resulted~~ results in changes of 0.6549–3.274 W m⁻² in SW_TOT in the five ocean regions (Table S2). The
370 SW_TOT responses ~~were~~ are the largest in the SP region, at 3.274 W m⁻², and 2.697 and 1.817 W m⁻² in
371 the NP and SA regions, respectively, while they were only 0.6549 and 0.7483 W m⁻² in the AsiaWP and
372 Equa regions, respectively. The injected sea-salt aerosols produced SW_TOT changes of 5.11–14.3 ~~15.22, 3~~
373 W m⁻² in the sensitive areas (Fig. 1b). Similarly, the increases in SW_TOT in the SP, SA, and NP regions
374 all exceeded 4.09 W m⁻², with the highest in the SP region at 15.22 14.3 W m⁻². In the AsiaWP and Equa
375 regions, although the increases in SW_TOT ~~were~~ are only 6.225.11 and 5.14 26 W m⁻², respectively, ~~it can~~
376 ~~still achieve the goal of offsetting the overall effective radiative forcing produced by anthropogenic~~
377 ~~activities in the sensitive areas. Also, when injecting at a uniform rate of 10^{-9} kg m⁻² s⁻¹ within the sensitive~~
378 ~~areas, for the entire region, the MCB efficiencies were greatly improved for all sea areas except Asia (Fig.~~
379 ~~S3).~~ Considering that the original intents of MCB or MSB design ~~were~~ are regional application (hurricane
380 mitigation, coral reef protection and polar sea ice recovery), (Latham et al., 2014), choosing to inject sea-

381 salt aerosols in the sensitive areas could achieve the corresponding cooling goals within the region, and
382 also affected larger areas through the diffusions and transports of aerosols. _

383 3.2 Characterization of the radiation responses.

384 SW_TOT responses ~~were~~are defined as the sum of the upward shortwave radiation flux response at the
385 TOA generated by the combined effects of the direct scattering effect of aerosols (SW_AER) and cloud
386 radiative effect (SW_CLD) after injecting sea-salt aerosols. Figure 4 shows the contributions of SW_AER
387 and SW_CLD responses in the SW_TOT produced by different injection ~~methods~~strategies in the five
388 ocean regions. The majority of the SW_TOT radiative flux response due to the ~~less injected~~lower mass
389 ~~injection~~ Natural $\times 5$ and Wind-adjusted strategies ~~was~~is caused by the SW_CLD response (Fig. 4 and
390 ~~Table 14a~~). In the NP, SP, and SA regions, the ~~contribution~~contributions of SW_CLD ~~exceeded~~exceed
391 70%, suggesting that sea-salt aerosols injected at these locations ~~increased~~increase the SW_TOT mainly
392 by affecting clouds through indirect effects. In the Equa, the responses of SW_TOT ~~were~~are entirely
393 caused by SW_AER. The proportion of SW_AER produced by the uniform injection of sea-salt aerosols
394 at a fixed rate of 10^{-9} kg m $^{-2}$ s $^{-1}$ continued to increase (Fig. 4c). In the ~~Asia~~WP, Equa, and SP regions, the
395 proportion of SW_AER exceeded that of SW_CLD. In the SA region, SW_CLD and SW_AER ~~were~~are
396 almost equal, while in the NP region, the SW_CLD response ~~was~~is 13.44 W m $^{-2}$, still greater than
397 SW_AER (9.708 W m $^{-2}$). This is because there ~~was~~is a saturation phenomenon in the cloud response to
398 aerosols injections (discussed below), and the NP, SP, and SA regions ~~provided~~provide more SW_CLD
399 responses, while the cloud responses in the ~~Asia~~WP and Equa regions ~~saturated~~saturate and no longer
400 ~~increased~~increase. The results of Fixed-wind-adjusted case show that, at the same injection amount, the
401 SW_AER responses caused by the injection ~~method~~strategy relying on wind speed ~~was~~is significantly
402 smaller than those of the method with fixed-rate uniform injection, while the disparity in SW_CLD
403 responses ~~was~~is minimal. This is because the injection ~~method~~strategy relying on wind speed distributed
404 most of the increased sea-salt aerosols to areas with already high emissions, such as strong-wind areas
405 and surf zones, where the excess marine aerosols ~~had~~have already saturated the cloud responses, resulting
406 in minor changes in SW_CLD. In areas with weak winds, the potentials for direct aerosol scattering
407 ~~were~~are not fully exploited due to the relatively small amounts of sea-salt aerosols injected, leading to a
408 lower SW_AER response.

409 Figures ~~S4S5~~ and ~~S5S6~~ show the spatial distributions of SW_CLD and SW_AER responses resulting
410 from different injection methods in the five ocean regions. The SW_CLD responses ~~were~~are stronger in

411 the three regions of NP, SP, and SA, while they ~~were~~are weaker in the regions of ~~Asia~~WP and Equa, and
412 in some grids they even led to a reduction of the upward shortwave radiation- (Fig. S5). The spatial
413 distributions of the SW_CLD responses ~~exhibited~~exhibit noticeable discontinuity, reflecting significant
414 regional differences in the non-uniform distributions of clouds and their impacts on shortwave radiation
415 at the TOA. The effect of cloud properties on SW_CLD will be shown in Section 3.5. Due to the influences
416 of various complex factors on cloud formations and distributions, simulation results related to clouds
417 show significant spatial variabilities. This might be the result of the combined effects of local
418 meteorological conditions and changes in cloud physical properties caused by sea-salt aerosol injections.

419 In contrast, the spatial distributions of the SW_AER response ~~were~~are smoother, leading to consistent
420 increases in upward shortwave radiation at the TOA in all ocean regions- (Fig. S6). This indicates smaller
421 spatial limitations in the distributions of aerosol particles, allowing direct scattering effects to take place
422 everywhere. The direct scattering effect of aerosols ~~was~~is primarily related to the concentrations and
423 physical properties of the particles (discussed below), unlike clouds, which ~~were~~are influenced by
424 multiple variables. These results suggest that when implementing geoengineering measures, it is essential
425 to comprehensively consider the interactions between aerosols and clouds, as well as their different
426 response patterns in various regions. Furthermore, the high spatial variabilities of cloud radiation effects
427 ~~emphasized~~emphasize the need for improved resolution in future model studies of cloud-aerosol
428 interactions.

429 The SW_CLD response resulting from the injection of sea-salt aerosols in the sensitive areas of five
430 ocean regions exhibits significant spatial differences. The SW_CLD response is larger than the SW_AER
431 response in the sensitive areas of NP, SP, and SA, indicating that the changes in SW_TOT are mainly
432 driven by the cloud radiation response (Fig. 5). In contrast, the SW_CLD response is smaller in the
433 ~~Asia~~WP and Equa regions. This regional difference is similar to that observed with uniform injection
434 across the entire region. The SW_AER response shows consistent results in all areas, resulting in a
435 radiation response change of ~~3.5558~~-~~5.4244~~ W m⁻² within the injection areas. In the ~~Asia~~WP and Equa,
436 the variations in SW_TOT ~~were~~are primarily driven by the direct scattering effects of aerosols.

437 Aerosols can have a greater impact on radiation responses outside the sensitive areas through
438 transports and diffusions, reaching up to three times the total radiation within the sensitive areas (Fig. 6).
439 In all regions except ~~Asia~~WP, the total SW_CLD response outside the sensitive region was about 270%-
440 408% higher than inside. In ~~Asia~~WP, the SW_CLD response outside the sensitive area ~~was only 29% of~~
441 ~~the response inside~~.has a negative effect. The SW_CLD responses in NP, SP, and SA ~~extended~~extend to

442 the west and northwest of the injection ~~areas~~by the prevailing winds, indicating that clouds in these areas
443 ~~were~~are affected by the injection of sea-salt aerosols (Fig. 5). Changes in cloud microphysical properties
444 ~~would~~will be presented later. The SW_CLD variations in other directions ~~were~~are not uniform, and there
445 ~~was~~is negative SW_CLD responses in some grids, which again reflected the spatial complexities of cloud
446 radiation effects. The direct scattering effects of aerosols on areas outside the sensitive region is reflected
447 in a widespread increase in upward shortwave radiation at the TOA. The total SW_AER responses outside
448 the sensitive areas in the five ocean regions ~~were~~are approximately 160%–281% higher than inside, but
449 lower than the impacts of SW_CLD responses outside the sensitive areas. There ~~were~~are consistencies in
450 the spatial distributions of SW_AER and SW_CLD responses.

451 3.3 Saturation of the cloud radiative responses.

452 Figure 7 shows that under low levels of sea-salt aerosol injections, radiation response changes ~~were~~are
453 mainly driven by SW_CLD responses. As the injected sea-salt aerosols increased, the SW_CLD responses
454 gradually ~~reached~~reach saturation. After reaching a certain injection level, the increases of SW_CLD
455 responses ~~stabilized~~stabilize at its maximum value and no longer increases with further injections. The
456 SW_CLD responses show large differences in the five ocean regions, and the different shapes and slopes
457 of the curves ~~indicated~~indicate that the cloud radiative forcing responses to the sea-salt aerosol injections
458 ~~were~~are different in each region. This might be due to variations in cloud types, cloud amounts, and
459 atmospheric conditions in the different regions. In the NP, SP, and SA, the SW_CLD responses
460 ~~exceeded~~exceed 10 W m^{-2} , while in AsiaWP, it ~~saturated~~saturates at 5 W m^{-2} . In Equa, when the sea-salt
461 aerosol injection rate ~~was~~is $10^{-9} \text{ kg m}^{-2} \text{ s}^{-1}$, the SW_CLD response ~~was~~is 0.545 W m^{-2} , and even when the
462 injection doubled, the SW_CLD response remained at 0.545 W m^{-2} . This implies that the SW_TOT at
463 Equa was almost exclusively from the contributions of the direct scattering effects of aerosols.

464 In contrast to SW_CLD, the SW_AER responses ~~increased~~increase linearly with the injections of
465 sea-salt aerosols ($R^2 > 0.99$). As the injection ~~increased~~increases, the contributions of SW_AER to
466 SW_TOT gradually ~~increased~~increase, surpassing the SW_CLD responses, and ~~showed~~show the same
467 trends across the five regions. This implies that at higher injection levels, the contributions of SW_CLD
468 to total radiation change saturated, and cloud properties no longer significantly ~~changed~~change. At this
469 point, sea-salt aerosols primarily ~~affected~~affect radiation through direct scattering effects, and the aerosol
470 particles' ability to scatter solar radiation continued to increase with the increases in aerosol quantities. In
471 some cloud-free regions or weather conditions, injected sea-salt aerosols ~~were~~are still able to function

472 through direct scattering.

473 There ~~existed~~exists a specific injection level at which the SW_CLD and SW_AER responses ~~were~~are
474 equal. In the NP region, when the injection level ~~was~~is approximately $1.55 \times 10^{-9} \text{ kg m}^{-2} \text{ s}^{-1}$, both SW_CLD
475 and SW_AER responses ~~were~~are 15 W m^{-2} . In the SP and SA, these levels ~~were~~are about $0.67 \times 10^{-9} \text{ kg m}^{-2} \text{ s}^{-1}$
476 and $1 \times 10^{-9} \text{ kg m}^{-2} \text{ s}^{-1}$, respectively. While in ~~Asia~~WP, the responses were already equal when the
477 injection amount was $0.15 \times 10^{-9} \text{ kg m}^{-2} \text{ s}^{-1}$. Since there ~~was~~is a saturation of the cloud radiation effects,
478 E_{MCB} ~~decreased~~decreases with the increases in sea-salt aerosol injection amounts (Fig. 7, red dashed line).
479 This can also explain the higher E_{MCB} of the Natural \times 5 and Wind-adjusted ~~methods~~strategies with
480 relatively low injection amounts (Fig. ~~3~~3b). Therefore, wind-dependent injection strategies led to the
481 injection of large amounts of sea-salt aerosols in certain areas with high wind speeds, leading to saturation
482 of cloud radiation effects, which might affect the performances of MCB in the simulations of regional
483 and global models.

484 When less sea-salt aerosols ~~were~~are injected, both SW_CLD and SW_AER responses
485 ~~contributed~~contribute to the changes of SW_TOT. As the injection amounts ~~increased~~increase, the
486 SW_CLD responses ~~saturated~~saturate, and the increases in SW_TOT depended on the increases in
487 SW_AER responses, leading to a decrease in E_{MCB} . (Fig. 7) Therefore, implementing geoengineering
488 with sea-salt aerosol injections required considering local atmospheric conditions and balancing the
489 relationships between cooling goals and sea-salt injection efficiencies.

490 Under clear and cloudless conditions, injecting sea-salt aerosols could still increase the SW_TOT
491 through direct scattering, and this effect ~~exceeded~~exceeds those of aerosol direct scattering when clouds
492 ~~were~~are present. The ~~variations~~variation of the upward shortwave radiation flux at the TOA under the
493 clear-sky conditions (SW_AER_CLR) ~~did~~does not exhibit significant regional heterogeneity across the
494 ocean areas (Figs. 5 and ~~S6~~S7), suggesting that the contribution of direct aerosol scattering ~~was~~is more
495 uniform globally when considering the effects of sea-salt injections on the Earth's radiation budget. The
496 SW_AER_CLR responses ~~were~~are also linearly correlated with the injection of sea-salt aerosols ($R^2 >$
497 0.99), and it ~~exceeded~~exceeds the SW_AER responses (Fig. 7). This is because cloud layers also
498 ~~scattered~~scatter and ~~absorbed~~absorb solar radiation, so this scattering effect ~~was~~is more significant under
499 clear sky conditions. It ~~was~~is reflected that in regions with strong cloud radiation effects, such as the NP,
500 SP, and SA regions, the differences between the SW_AER and SW_AER_CLR responses ~~were~~are also
501 larger (Fig. 7). When injecting sea-salt aerosol in sensitive areas, the spatial distributions of
502 SW_AER_CLR and SW_AER responses ~~were~~are highly consistent (Fig. 5). Therefore, injecting sea-salt

503 aerosol under conditions of low cloud covers or clear skies also ~~increased~~increases the upward shortwave
504 radiation flux at the TOA.

505 3.4 Factors affecting the radiation effects.

506 ~~The direct radiative effect of aerosols is mainly determined by their own optical properties. In WRF-~~
507 ~~CMAQ, the emitted sea salt aerosol particle size distributions were adjusted to the local relative humidity~~
508 ~~(Kelly et al., 2010; Zhang et al., 2005). The dry diameter of sea salt aerosols injected into the five regions~~
509 ~~was about 0.11–0.15 μm (Figs. 1a and S7), and the wet diameter was about 0.22–0.3 μm (Fig. S8). The~~
510 ~~single scattering albedo (SSA) of aerosols describes the ratio of aerosol particles' ability to absorb and~~
511 ~~scatter solar radiations. After the injection of sea salt aerosols, the SSA of the accumulation mode aerosols~~
512 ~~in the five regions generally increased by about 0.003–0.005, and in some regions within the area, the~~
513 ~~SSA increased by over 0.007, with an average increase of 0.001–0.003 in sensitive areas (Fig. S9). This~~
514 ~~indicates that the injected sea salt aerosol particles could scatter sunlight more effectively than absorb it,~~
515 ~~causing solar radiation to be reflected back into space. The asymmetry factor of aerosols is a parameter~~
516 ~~describing the directionality of aerosol particle scattering of sunlight, and an important factor for~~
517 ~~evaluating direct aerosol radiative forcing (Zhao et al., 2018). The injection of sea salt aerosols in the five~~
518 ~~regions reduced the asymmetry factor by 0.007–0.029, with an average reduction of 0.01–0.027 in~~
519 ~~sensitive areas (Fig. S10). This indicates that the injected sea salt aerosols tended to scatter more~~
520 ~~uniformly or backward rather than in a forward direction.~~

521 Uniform injections of 10^{-9} kg m⁻² s⁻¹ sea-salt aerosols led to an increase in aerosol optical depth (AOD) of
522 ~~0.220~~–0.37 in all regions (Fig. 8). The distributions of AOD within the regions ~~were~~are not uniform due
523 to aerosol transports and diffusions, with some areas showing an increase in AOD of over 0.6. Injecting
524 sea-salt aerosols in sensitive areas ~~led~~lead to an AOD increase of ~~0.08077~~–0.12, while outside the
525 injection areas, AOD gradually ~~decreased~~decreases as the aerosols ~~were transported~~transport and
526 ~~dispersed~~disperse. With the increases in sea-salt aerosol injections, AOD ~~showed~~shows a linear increase
527 within a certain range in all five ocean regions ($R^2 > 0.997$, Fig. 9a). There ~~was~~is a strong correlation
528 between the AOD changes caused by sea-salt injection and the SW_AER responses. When sea-salt
529 aerosols ~~were~~are uniformly injected across the entire region, the correlation coefficients between AOD
530 and SW_AER responses in the five ocean areas ~~were~~are greater than 0.94, and when injected in sensitive
531 areas, the correlation coefficients ~~were~~are greater than 0.99 (Fig. ~~S8~~, ~~S11~~). ~~There was also a strong spatial~~
532 ~~consistency between~~The optical properties of injected aerosols are described in Supplementary Text S2.

设置了格式: 字体: 五号

带格式的: 缩进: 首行缩进: 0 字符

设置了格式: 字体: 五号

533 ~~In general, the spatial distribution of AOD injected sea-salt aerosols scatter sunlight more efficiently than~~
534 ~~absorb it, causing solar radiation to be reflected back into space and SW_AER response (Fig. S5, third~~
535 ~~row, and Fig. 8, second column; Fig. 5, second column, and Fig. 8, third column) tend to scatter more~~
536 ~~uniformly or backward rather than forward.~~

537 ~~There were significant differences in the distributions of clouds in the five ocean regions during the~~
538 ~~study period, with wide distributions of liquid clouds in the NP, SP and SA regions, and less clouds in~~
539 ~~Asia and Equa. The cloud heights were distributed between 500–2000 meters, centered around 1000~~
540 ~~meters (Figs. S12 and S14). In the regions with higher cloud cover, such as NP, SP, and SA, injected sea-~~
541 ~~salt aerosols significantly increased/increases cloud fraction, (Fig. 2, third column and Table 1), leading to~~
542 ~~the formations of more clouds or expanding the coverage, vertical thickness and lifetime of existing~~
543 ~~clouds (Goddard et al., 2022). The injection of sea-salt aerosols in sensitive areas had/have similar results,~~
544 ~~where cloud fractions increased/increase both inside the injection areas and in the regions affected by~~
545 ~~aerosol transports and diffusions (Fig. S13).~~

546 ~~The injected sea salt aerosols affected the cloud microphysical properties through indirect effects,~~
547 ~~thereby influencing cloud radiative responses.~~ Taking the SP region as an example, Fig. 10 demonstrates
548 that uniformly injections of 10^{-9} kg m⁻² s⁻¹ sea-salt aerosols significantly increased/increases the CDNC.
549 More cloud droplets captured/capture more water vapor, leading to an increase in liquid water path (LWP).
550 Additionally, the increases in cloud thickness also contributed/contribute to the increase in LWP. The
551 increases/increase in CDNC decreased/decreases the mean r_e by 8.9 μm (~ -37%), increased/increases the
552 cloud optical thickness (COT) by more than 220%, and ultimately increased/increases the mean cloud
553 albedo over the region by 0.19 (~64%). Similarly, injecting sea-salt aerosols in the NP and SA regions led
554 to average cloud albedo increases of 0.17 and 0.20, respectively, while in the AsiaWP and Equa, the
555 increases were/are 0.15 and 0.13, respectively (Figs. S15–S18/S14–S17). The injections/injection of sea-
556 salt aerosols within the sensitive areas had/has less effect on cloud microphysical properties than the whole
557 region injections. This is because when sea-salt aerosols were/are injected across the entire region, the
558 surrounding sea-salt aerosols affected/affect the sensitive areas through transports, resulting in an
559 enhanced cumulative effect on cloud microphysical properties in the sensitive areas. Injecting sea-salt
560 aerosol in the sensitive area of the SP affected clouds in the surrounding region through transports,
561 increased/increases the average cloud albedo across the entire area by 0.03/0.32 over the entire region and
562 by 0.12 within the sensitive regions, which was/is less than the effects of injection across the entire area
563 (Fig. S19/S18). Similarly, injecting sea-salt aerosols in the sensitive areas of other sea/ocean regions led/lead

564 to average cloud albedo increases of ~~0.04~~0.015–~~0.02~~0.024 across the entire area, with increases of 0.11 in the
565 sensitive areas of the SP and SA regions, and increases of ~~0.09~~0.090 and 0.10 in the AsiaWP and Equa,
566 respectively (Figs. ~~S20–S23~~S19–S22).

567 3.5 Drivers of SW_CLD responses.

568 The cloud radiation forcing (CRF) parameters ~~were~~are used to calculate the effects of changes in cloud
569 cover and cloud albedo on the SW_CLD responses due to the injections of sea-salt aerosols. Figure
570 ~~S24~~S23 illustrates the increase in the CRF parameter coinciding with the increases in the SW_CLD
571 responses after uniform injection of sea-salt aerosols in the five regions (Fig. ~~S4~~S5, third row). The results
572 ~~were~~are similar for injections in the sensitive areas (Fig. ~~S25~~S24, third column, and Fig. 5, first column).
573 The CRF'_{param} calculated using the perturbation method indicates that in the five ocean regions, CRF'_{param}
574 ~~was~~is primarily driven by perturbations in cloud albedo (Fig. ~~S26~~S25, first column), and it significantly
575 ~~surpassed~~surpasses the changes in cloud fractions and their interactions. Cloud albedo changes
576 ~~explained~~explain over 70% of the CRF'_{param} in all ~~four~~five regions except the Equa. The
577 ~~contributions~~contribution of cloud fraction changes ~~ranged~~ranges from 13.9% to 23.87%, while the
578 interactions between the two factors ~~accounted~~account for only about 10% (Fig. ~~S26~~S25, second and third
579 columns). The results ~~were~~are similar for injections in sensitive regions, where changes in cloud albedo
580 accounted for ~~68.9%–79.6~~58.8%–99.4% of the CRF'_{param}, followed by changes in cloud fractions, with
581 the smallest contributions from their interactions (Fig. ~~S27~~S26).

582 Figure 11 evaluates the relative effects of Twomey, LWP, and cloud fractions on the SW_CLD
583 responses after uniformly injecting sea-salt aerosols in five ocean regions. The results indicate that
584 changes in CDNC (Twomey effect) and LWP ~~were~~are the main drivers of SW_CLD responses, while
585 changes in cloud fraction ~~contributed~~contribute minimally to the SW_CLD responses. Except for the
586 Equa region, changes in CDNC and LWP accounted for 48.24%–52.45% and ~~38.9~~39.0%–41.97% of the
587 SW_CLD changes, respectively, with cloud fraction changes contributing to less than 10%~~.0%~~ (Fig. 11).
588 The results ~~were~~are similar for injections in sensitive areas, with changes in CDNC and LWP contributing
589 similarly and more than changes in cloud fractions to SW_CLD (Fig. ~~S28~~S27). The changes in SW_CLD
590 responses after aerosol injections in the sensitive areas of Equa ~~were~~are mainly contributed by LWP
591 effects (~70%).

592 Uniform injections of sea-salt aerosols at a rate of 10^{-9} kg m⁻² s⁻¹ produced susceptibilities ($\frac{\Delta\alpha}{\Delta\ln AOD}$)
593 ranging from ~~0.0003~~0.0030 to 0.0035 in the five regions, with corresponding spatial distributions shown

594 in Fig. 11. NP, SP, and SA regions ~~exhibited~~exhibit cloud responses that ~~were~~are more sensitive to aerosol
595 injections in most of the region, with susceptibilities ranging from 0.0028 to 0.0035. The Equa
596 ~~showed~~shows the lowest susceptibility, indicating that the system ~~was~~is less responsive to variations in
597 aerosol injections. It is noteworthy that although the average susceptibility in the AsiaWP region ~~was~~is
598 0.0013, the higher susceptibility values ~~were~~are concentrated in the north of 35°N, where the average
599 susceptibility ~~was~~is 0.0026, similar to those of the SP region, suggesting that clouds here ~~were~~are more
600 susceptible to aerosol injections. Injecting sea-salt aerosols in sensitive areas mostly ~~resulted~~results in
601 cloud that ~~were~~are located outside the sensitive areas (Fig. ~~S28~~S27). Injecting sea-salt aerosols in the
602 sensitive areas of SP and SA ~~had~~have a greater impact on the northwest. In the sensitive areas of NP,
603 injecting sea-salt aerosols ~~had~~have a larger impact on the west. In the AsiaWP, the injection of sea-salt
604 aerosols into the sensitive area ~~did~~does not fully reflect its susceptibility because we ~~had~~choose
605 to calculate the sensitive areas away from the boundary, and the greatest susceptibilities in the AsiaWP
606 region ~~happened~~happens to be in the northern part of the region near the boundary.

607 4. Discussions and conclusions

608 Many studies have discussed the contributions of both the direct and indirect effects of MCB. Some
609 studies suggest that MCB primarily relies on the indirect effects, as originally conceived, i.e., injecting
610 aerosols to brighten clouds (Jones and Haywood, 2012; Latham et al., 2012). ~~On the other hand,~~
611 ~~other~~Other studies proposed that the direct scattering effects of aerosols may be more important (Ahlm et
612 al., 2017; Kravitz et al., 2013; Mahfouz et al., 2023; Niemeier et al., 2013; Partanen et al., 2012). Our
613 results indicate that the ~~importance~~importances of both aerosol direct and indirect effects during MCB
614 implementation ~~depended~~depend on the injection ~~amounts~~strategies and the choice of injection regions.
615 In cases of low sea-salt aerosol injections or the early stage of MCB implementations, changes in radiative
616 response ~~were~~are mainly driven by indirect effects, causing clouds to brighten easily. As the
617 ~~injections~~injection of sea-salt aerosol ~~increased~~increases, the radiative ~~effects~~effect on clouds
618 ~~saturated~~saturates, and the clouds ~~were~~are difficult to brighten. In contrast, the direct effect continued to
619 increase linearly, leading to a subsequent decrease in the efficiencies of MCB. ~~Partanen et al.~~
620 ~~(2012)~~Partanen et al. (2012) first considered the relative importance of aerosol direct and indirect effects
621 in MCB and preliminarily found the saturated non-linear phenomenon of indirect effects at high CDNC,
622 as well as the linear relationships between direct effects and injection amounts. ~~Haywood et al.~~
623 ~~(2023)~~Haywood et al. (2023) also found a decrease in MCB efficiency with increasing aerosol injections.

624 Regions initially susceptible to modification gradually became less susceptible, and aerosol direct
625 radiation effects dominated. ~~This study emphasized and quantified these findings~~Other use General
626 Circulation Model (GCM) studies also found similar results (Alterskjær and Kristjánsson, 2013; Rasch et
627 al., 2024; Stjern et al., 2018). This study highlights and quantifies these findings in a regional model for
628 the first time, showing the changing trends of direct and indirect effects with injection amounts in the
629 different ocean regions. ~~The best results were~~Also due to the higher resolution of the regional model, this
630 study provides more detailed cloud component changes due to sea-salt aerosol injection. The best results
631 are obtained in regions with persistent stratocumulus clouds (e.g., the oceans along the west coast of the
632 continent), where the injected sea-salt aerosols ~~worked~~work together through both direct and indirect
633 effects. However, in cloud-free or less cloudy regions, MCB implementation can achieve the goal of
634 reflecting more sunlight through the direct scattering effect of aerosols. Considering the uncertainty in
635 the model's resolution of clouds and the fact that, in reality, the cloud distributions ~~were~~are also greatly
636 influenced by the local meteorological conditions, the direct scattering effects of sea-salt aerosols on MCB
637 contributions ~~were~~are relatively certain. Therefore, in cloud-free or less cloudy regions, the direct
638 ~~effects~~effect of aerosols ~~become~~becomes more important.

639 In the early stages of Earth-System modeling studies, the MCB processes were often simulated by
640 presetting $CDNC = 375$ or 1000 cm^{-3} in the lower regions of the ocean (Jones et al., 2009; Latham et al.,
641 2008; Rasch et al., 2009). However, many follow-up studies have suggested that injections of sea-salt
642 aerosols were difficult to produce a uniform CDNC field due to aerosol dilutions, depositions, and the
643 dependences of the spray rate on wind speed. The CDNC ~~was~~is highly variable spatially, and studies have
644 even reported reductions in CCN and CDNC caused by the injections of sea-salt aerosols (Alterskjær et
645 al., 2012; Korhonen et al., 2010; Pringle et al., 2012). In this study, after injecting accumulation mode
646 sea-salt aerosols at a rate of $10^{-9} \text{ kg m}^{-2} \text{ s}^{-1}$, the average CDNC concentrations for five ocean regions
647 ~~ranged~~range from ~~60.2~~ to ~~103.100~~ cm^{-3} , and the spatial distributions ~~were~~are uneven (Fig. 10 and Figs.
648 ~~S15–S18~~S14–S17). Figure 9b indicates that the ~~CCN~~CCNs in the five regions ~~increased~~increase linearly
649 ($R^2 = 1$) with increasing sea-salt aerosol injections, but not all of the ~~CCN~~CCNs ~~are~~are converted to
650 cloud droplets. After doubling the injection amounts, the regional average CDNC ~~was~~ ~~85–134~~is ~~84.8–130~~
651 cm^{-3} , with only some grid points exceeding 200 cm^{-3} within the regions. This implies that injecting more
652 sea-salt aerosols at this point ~~did~~does not result in more cloud droplets, and the conversion of CCN into
653 cloud droplets ~~was~~is less efficient, which ~~slowed~~slows the CDNC growths and ~~tended~~tends to saturation
654 (Fig. 9c). ~~Alterskjær et al. (2012)~~Alterskjær et al. (2012) similarly injected sea-salt aerosols at a rate of

设置了格式: 字体: (默认) 宋体, 四号, (国际) + 西文正文 (等
线), 英语(美国)

655 $10^{-9} \text{ kg m}^{-2} \text{ s}^{-1}$ and found that despite emitting sea-salt mass 70 times larger than suggested by Latham et
656 al. (2008), the average CDNC over the ocean was below their assumed value of 375 cm^{-3} . This is mainly
657 due to increased competitive effects, decreased maximum supersaturations, inhibitions of aerosol
658 activations, and closures of SO_4 nucleation, resulting in reduced effectiveness of sea salt
659 injections. Latham et al. (2008), the average CDNC over the ocean was below their assumed value of 375
660 cm^{-3} . This is mainly due to increased competitive effects, decreased maximum supersaturations,
661 inhibitions of aerosol activations, and closures of SO_4 nucleation, resulting in reduced effectiveness of
662 sea salt injections. Notably, however, Wood (2021) found that decreased activation due to competition
663 may be overestimated in the Abdul-Razzak and Ghan activation parameterization used in many GCMs
664 relative to a parcel model. When Partanen et al. (2012) injected sea-salt aerosols in a Wind-adjusted way
665 (injection amount different from this study), they found the CDNC values of 596, 650, and 784 cm^{-3} in
666 the NP, SP, and SA regions, respectively. Injecting smaller-sized sea-salt aerosols even yielded CDNC
667 values exceeding 1000 cm^{-3} . They concluded that such high values were mainly due to the model's
668 overestimation of the sizes and solubilities of accumulated mode particles, with some non-activated
669 particles forming cloud droplets. Hill and Ming (2012) increased the concentrations of sea-salt aerosols
670 by a factor of five, resulting in an average CDNC increasing from 68 to 148 cm^{-3} between 850–925 hPa.
671 It is noteworthy that Hill and Ming (2012) increased all modes
672 of sea-salt aerosols, while this study only injected accumulation mode sea-salt aerosols. Many studies
673 have reported that selecting the appropriate injection particle size was crucial for MCB (Andrejczuk et
674 al., 2014; Hoffmann and Feingold, 2021; Partanen et al., 2012), and injecting Aitken and coarse modes
675 may even lead to a positive forcing with CDNC decreasing (Alterskjær and Kristjánsson, 2013). However,
676 Wood (2021) argued that particles with a geometric mean dry diameter of 30–60 nm were most effective
677 in brightening cloud layers, and Goddard et al. (2022) similarly found that injecting Aitken mode sea-salt
678 aerosols generated larger radiative flux changes compared to accumulation mode (8.4 W m^{-2} versus 3.1
679 W m^{-2}). There were still considerable discussions about choosing the appropriate aerosol particle sizes
680 during the implementation of MCB, with different models and parameterization schemes providing
681 different recommendations. The sensitivity of MCB to particle size was not considered in this paper and
682 was left for future research.

683 In this study, the injection of $10^{-9} \text{ kg m}^{-2} \text{ s}^{-1}$ accumulation mode sea-salt aerosols increased increases
684 cloud albedo in the five ocean regions by 0.13–0.20, with a maximum of more than 0.3. After doubling
685 the injection amounts, the regional average cloud albedo could reach 0.45–0.55, representing a cloud

686 albedo change of 0.15–0.24 (Fig. 9d). These values ~~achieved~~ achieve the targeted cloud albedo change as
687 envisioned in previous studies. Bower et al. (2006) suggested that to compensate for the warming
688 associated with doubling atmospheric CO₂ concentrations, a cloud albedo change of 0.16 was needed in
689 three stratocumulus cloud regions (off the west coast of Africa and North and South America, representing
690 3% of global cloud cover). Wood (2021) proposed seeding Aitken mode particles in approximately 9% of
691 the ocean to achieve a corresponding cloud albedo increase of 0.16. It was also suggested that injecting
692 sea-salt aerosols in a clean, undisturbed state would produce more brightening. Fig. 9d confirms this
693 finding, indicating that clouds are more likely to brighten in the early stages of sea-salt aerosol injection,
694 and the efficiency of cloud brightening decreases with increasing injection amounts. ~~Kravitz et al. (2014)~~
695 ~~achieved a maximum cloud albedo change of 0.23 by injecting CCN in the Arctic region.~~ ~~Goddard et al.~~
696 ~~(2022), simulating injecting accumulation mode sea-salt aerosols in the central Gulf of Mexico, achieved~~
697 ~~a simulated cloud albedo change of approximately 0.1 in the main impact region, while switching to~~
698 ~~Aitken mode injection resulted in a cloud albedo change of up to 0.35.~~ For the global implementation of
699 MCB, global cloud albedo increases of 0.02 (Bower et al., 2006), 0.062 (Latham et al., 2008), or 0.074
700 (Lenton and Vaughan, 2009) were estimated. ~~The change in cloud albedo is influenced by the properties~~
701 ~~of injected particles and the injection strategies.~~ ~~Jenkins et al. (2013) proposed that the optimal injection~~
702 ~~time should be in the early morning over weakly precipitating cloud regions, achieving a cloud albedo~~
703 ~~increase of 0.28.~~ ~~Goddard et al. (2022), simulating injecting accumulation mode sea-salt aerosols in the~~
704 ~~central Gulf of Mexico, and achieved a simulated cloud albedo change of approximately 0.1 in the main~~
705 ~~impact region, while switching to Aitken mode injection resulted in a cloud albedo change of up to 0.35.~~

706 The contributions of the change in cloud fractions to the SW_CLD responses in this study ~~were~~ are
707 small, which ~~was~~ is consistent with the results of ~~Goddard et al. (2022)~~ ~~Goddard et al. (2022)~~. However,
708 many observational studies indicate that the contribution of cloud fraction to the shortwave radiative
709 forcing should be similar to those of the CDNC and LWP (Chen et al., 2014; Rosenfeld et al., 2019).
710 ~~Goddard et al. (2022)~~ ~~Goddard et al. (2022)~~ believe that this was due to the fact that the regional
711 atmosphere was wetter during the simulation periods and that the relative contributions of changes in
712 cloud fraction to the SW_CLD response would be expected to increase in drier months (~~Fig. S29~~). Three
713 of the five ocean regions in this study (~~SA, SP, and NP~~) ~~were~~ are much drier and more stable than the
714 Gulf of Mexico simulated by ~~Goddard et al. (2022)~~ ~~Goddard et al. (2022)~~ (Fig. S28). Furthermore, when
715 we switched to conducting the experiments again in the dry months of the same year, the contribution of
716 cloud fraction to SW_CLD did not change much, remaining at ~10% (Fig. S28). We believe that this

717 might be a difference due to the parameterization scheme or resolution of the model. [Liu et al. \(2020\)](#) [Liu](#)
718 [et al. \(2020\)](#) simulated with WRF–Chem model and found that the cloud fraction susceptibilities to
719 aerosols in Morrison scheme and the Lin scheme were only about half of those observed by Moderate
720 Resolution Imaging Spectroradiometer (MODIS). The neglected sub-gridded clouds in the 12-km
721 resolution simulations might lead to an underestimation of the radiative effects of clouds ([Yu et al., 2014](#)).
722 In addition, cloud fractions ~~were~~[are](#) more commonly underestimated in the model ([Glotfelty et al., 2019](#)),
723 and using an updated parameterization scheme that accounts for sub-grid condensation might improve
724 the model's ability to resolve clouds ([Zhao et al., 2023](#)). The effects of finer resolution and more
725 parameterization schemes on aerosol-cloud interactions still need to be verified. Considering the
726 difficulties of modeling to accurately capture the effects of cloud fractions on radiation, the actual effects
727 of MCB may be underestimated. ~~The radiative results obtained in this study may represent a lower limit~~
728 ~~to cooling.~~

729 This study ~~provided~~[provides](#) quantifiable data on cloud and radiation changes for the implementation
730 of MCB over the regional oceans, and an optimization scheme on the injection strategy by adjusting the
731 injection amounts and selecting sensitive areas. It is noteworthy that different parameterization schemes,
732 models, and resolutions can influence results, especially the cloud feedback on the injected sea-salt
733 aerosols, which is a major reason for discrepancies between models ([Stjern et al., 2018](#)). ~~In Earth-system~~
734 ~~model studies, there has been a rich discussion of the climate and ecological impacts of the MCB with~~
735 ~~the Geoengineering Model Intercomparison Project (GeoMIP) under the same framework.~~~~In Earth-~~
736 ~~system model studies, there has been a rich discussion of the climate and ecological impacts of the MCB~~
737 ~~with the same framework under the Geoengineering Model Intercomparison Project (GeoMIP) ([Rasch et](#)~~
738 ~~al., 2024).~~ However, there is still a lack of a unified framework for mid-scale MCB research.

设置了格式: 英语(美国)

741 **Data and code availability**

742 The computational code for cloud and radiation can be found in the code publicly available from [Goddard](#)
743 ~~et al. (2022)~~[Goddard et al. \(2022\)](#). The model results are available upon request.

744 **Supplemental information.**

745 The supplementary information related to this article is available online.

746 **Competing interests.** The authors declare that they have no conflict of interest.

747 **Acknowledgements.** The study was motivated by the need to assess the susceptibility of clouds over
748 locations such as the Great Barrier Reef, where a marine cloud brightening experiment is being performed
749 by the Reef Restoration and Adaptation Program of the Southern Cross University. The authors would
750 like to thank P. B. Goddard for his open-source computing methods and codes.

751 **Financial supports.** This work was supported by National Natural Science Foundation of China (No.
752 72361137007, 42175084, 21577126, 41561144004), Ministry of Science and Technology of China (No.
753 2016YFC0202702, 2018YFC0213506, 2018YFC0213503) and National Air Pollution Control Key Is-
754 sues Research Program (No. DQGG0107).

756 **References**

757 Ahlm, L., Jones, A., Stjern, C. W., Muri, H., Kravitz, B., and Kristjánsson, J. E.: Marine cloud brightening – as effective
758 without clouds, *Atmospheric Chemistry and Physics*, 17, 13071–13087, <https://doi.org/10.5194/acp-17-13071-2017>,
759 2017.

760 Albrecht, B. A.: Aerosols, Cloud Microphysics, and Fractional Cloudiness, *Science*, 245, 1227–1230,
761 <https://doi.org/10.1126/science.245.4923.1227>, 1989.

762 Alterskjær, K. and Kristjánsson, J. E.: The sign of the radiative forcing from marine cloud brightening depends on both
763 particle size and injection amount, *Geophysical Research Letters*, 40, 210–215, <https://doi.org/10.1029/2012GL054286>,
764 2013.

765 Alterskjær, K., Kristjánsson, J. E., and Seland, Ø.: Sensitivity to deliberate sea salt seeding of marine clouds –
766 observations and model simulations, *Atmospheric Chemistry and Physics*, 12, 2795–2807, [https://doi.org/10.5194/acp-](https://doi.org/10.5194/acp-12-2795-2012)
767 12-2795-2012, 2012.

768 Andrejczuk, M., Gadian, A., and Blyth, A.: Numerical simulations of stratocumulus cloud response to aerosol
769 perturbation, *Atmospheric Research*, 140–141, 76–84, <https://doi.org/10.1016/j.atmosres.2014.01.006>, 2014.

770 Binkowski, F. S. and Roselle, S. J.: Models-3 Community Multiscale Air Quality (CMAQ) model aerosol component 1.
771 Model description, *Journal of Geophysical Research: Atmospheres*, 108, <https://doi.org/10.1029/2001JD001409>, 2003.

772 Bower, K., Choulaton, T., Latham, J., Sahraei, J., and Salter, S.: Computational assessment of a proposed technique for
773 global warming mitigation via albedo-enhancement of marine stratocumulus clouds, *Atmospheric Research*, 82, 328–

774 336, <https://doi.org/10.1016/j.atmosres.2005.11.013>, 2006.

775 Carlton, A. G. and Baker, K. R.: Photochemical Modeling of the Ozark Isoprene Volcano: MEGAN, BEIS, and Their
776 Impacts on Air Quality Predictions, *Environ. Sci. Technol.*, 45, 4438–4445, <https://doi.org/10.1021/es200050x>, 2011.

777 Chen, Y.-C., Christensen, M. W., Xue, L., Sorooshian, A., Stephens, G. L., Rasmussen, R. M., and Seinfeld, J. H.:
778 Occurrence of lower cloud albedo in ship tracks, *Atmospheric Chemistry and Physics*, 12, 8223–8235,
779 <https://doi.org/10.5194/acp-12-8223-2012>, 2012.

780 Chen, Y.-C., Christensen, M. W., Stephens, G. L., and Seinfeld, J. H.: Satellite-based estimate of global aerosol–cloud
781 radiative forcing by marine warm clouds, *Nature Geosci.*, 7, 643–646, <https://doi.org/10.1038/ngeo2214>, 2014.

782 Christensen, M. W., Jones, W. K., and Stier, P.: Aerosols enhance cloud lifetime and brightness along the stratus-to-
783 cumulus transition, *Proceedings of the National Academy of Sciences*, 117, 17591–17598,
784 <https://doi.org/10.1073/pnas.1921231117>, 2020.

785 Forster, P., Ramaswamy, V., Artaxo, P., Berntsen, T., Betts, R., Fahey, D. W., Haywood, J., Lean, J., Lowe, D. C., Raga,
786 G., Schulz, M., Dorland, R. V., Bodeker, G., Etheridge, D., Foukal, P., Fraser, P., Geller, M., Joos, F., Keeling, C. D.,
787 Keeling, R., Kinne, S., Lassey, K., Oram, D., O’Shaughnessy, K., Ramankutty, N., Reid, G., Rind, D., Rosenlof, K.,
788 Sausen, R., Schwarzkopf, D., Solanki, S. K., Stenchikov, G., Stuber, N., Takemura, T., Textor, C., Wang, R., Weiss, R.,
789 Whorf, T., Nakajima, T., Ramanathan, V., Ramaswamy, V., Artaxo, P., Berntsen, T., Betts, R., Fahey, D. W., Haywood,
790 J., Lean, J., Lowe, D. C., Myhre, G., Nganga, J., Prinn, R., Raga, G., Schulz, M., and Dorland, R. V.: Changes in
791 Atmospheric Constituents and in Radiative Forcing, 2007.

792 Ghan, S. J., Liu, X., Easter, R. C., Zaveri, R., Rasch, P. J., Yoon, J.-H., and Eaton, B.: Toward a Minimal Representation
793 of Aerosols in Climate Models: Comparative Decomposition of Aerosol Direct, Semidirect, and Indirect Radiative
794 Forcing, *Journal of Climate*, 25, 6461–6476, <https://doi.org/10.1175/JCLI-D-11-00650.1>, 2012.

795 Glotfelty, T., Alapaty, K., He, J., Hawbecker, P., Song, X., and Zhang, G.: The Weather Research and Forecasting Model
796 with Aerosol–Cloud Interactions (WRF-ACI): Development, Evaluation, and Initial Application, *Mon Weather Rev.*, 147,
797 1491–1511, <https://doi.org/10.1175/MWR-D-18-0267.1>, 2019.

798 Goddard, P. B., Kravitz, B., MacMartin, D. G., and Wang, H.: The Shortwave Radiative Flux Response to an Injection
799 of Sea Salt Aerosols in the Gulf of Mexico, *Journal of Geophysical Research: Atmospheres*, 127, e2022JD037067,
800 <https://doi.org/10.1029/2022JD037067>, 2022.

801 Gong, S. L.: A parameterization of sea-salt aerosol source function for sub- and super-micron particles, *Global
802 Biogeochemical Cycles*, 17, <https://doi.org/10.1029/2003GB002079>, 2003.

803 Grythe, H., Ström, J., Krejci, R., Quinn, P., and Stohl, A.: A review of sea-spray aerosol source functions using a large
804 global set of sea salt aerosol concentration measurements, *Atmospheric Chemistry and Physics*, 14, 1277–1297,
805 <https://doi.org/10.5194/acp-14-1277-2014>, 2014.

806 Haywood, J. M., Jones, A., Jones, A. C., and Rasch, P. J.: Climate Intervention using marine cloud brightening (MCB)
807 compared with stratospheric aerosol injection (SAI) in the UKESM1 climate model, *EGU sphere*, 1–38,
808 <https://doi.org/10.5194/egusphere-2023-1611>, 2023.

809 Hill, S. and Ming, Y.: Nonlinear climate response to regional brightening of tropical marine stratocumulus, *Geophysical
810 Research Letters*, 39, <https://doi.org/10.1029/2012GL052064>, 2012.

811 Hoffmann, F. and Feingold, G.: Cloud Microphysical Implications for Marine Cloud Brightening: The Importance of the
812 Seeded Particle Size Distribution, *Journal of the Atmospheric Sciences*, 78, 3247–3262, [https://doi.org/10.1175/JAS-D-](https://doi.org/10.1175/JAS-D-21-0077.1)
813 [21-0077.1](https://doi.org/10.1175/JAS-D-21-0077.1), 2021.

814 Horowitz, H. M., Holmes, C., Wright, A., Sherwen, T., Wang, X., Evans, M., Huang, J., Jaeglé, L., Chen, Q., Zhai, S.,
815 and Alexander, B.: Effects of Sea Salt Aerosol Emissions for Marine Cloud Brightening on Atmospheric Chemistry:
816 Implications for Radiative Forcing, *Geophysical Research Letters*, 47, e2019GL085838,
817 <https://doi.org/10.1029/2019GL085838>, 2020.

818 Janssens-Maenhout, G., Crippa, M., Guizzardi, D., Dentener, F., Muntean, M., Pouliot, G., Keating, T., Zhang, Q.,
819 Kurokawa, J., Wankmüller, R., Denier van der Gon, H., Kuenen, J. J. P., Klimont, Z., Frost, G., Darras, S., Koffi, B., and
820 Li, M.: HTAP_v2.2: a mosaic of regional and global emission grid maps for 2008 and 2010 to study hemispheric transport
821 of air pollution, *Atmospheric Chemistry and Physics*, 15, 11411–11432, <https://doi.org/10.5194/acp-15-11411-2015>,
822 2015.

823 ~~Jenkins, A. K. L., Forster, P. M., and Jackson, L. S.: The effects of timing and rate of marine cloud brightening aerosol~~
824 ~~injection on albedo changes during the diurnal cycle of marine stratocumulus clouds, *Atmospheric Chemistry and*~~
825 ~~*Physics*, 13, 1659–1673, <https://doi.org/10.5194/acp-13-1659-2013>, 2013.~~

826 Jones, A. and Haywood, J. M.: Sea-spray geoengineering in the HadGEM2-ES earth-system model: radiative impact and
827 climate response, *Atmospheric Chemistry and Physics*, 12, 10887–10898, <https://doi.org/10.5194/acp-12-10887-2012>,
828 2012.

829 Jones, A., Haywood, J., and Boucher, O.: Climate impacts of geoengineering marine stratocumulus clouds, *Journal of*
830 *Geophysical Research: Atmospheres*, 114, <https://doi.org/10.1029/2008JD011450>, 2009.

831 Kelly, J. T., Bhave, P. V., Nolte, C. G., Shankar, U., and Foley, K. M.: Simulating emission and chemical evolution of
832 coarse sea-salt particles in the Community Multiscale Air Quality (CMAQ) model, *Geoscientific Model Development*,
833 3, 257–273, <https://doi.org/10.5194/gmd-3-257-2010>, 2010.

834 Korhonen, H., Carslaw, K. S., and Romakkaniemi, S.: Enhancement of marine cloud albedo via controlled sea spray
835 injections: a global model study of the influence of emission rates, microphysics and transport, *Atmospheric Chemistry*
836 *and Physics*, 10, 4133–4143, <https://doi.org/10.5194/acp-10-4133-2010>, 2010.

837 Kravitz, B., Forster, P. M., Jones, A., Robock, A., Alterskjær, K., Boucher, O., Jenkins, A. K. L., Korhonen, H.,
838 Kristjánsson, J. E., Muri, H., Niemeier, U., Partanen, A.-I., Rasch, P. J., Wang, H., and Watanabe, S.: Sea spray
839 geoengineering experiments in the geoengineering model intercomparison project (GeoMIP): Experimental design and
840 preliminary results, *Journal of Geophysical Research: Atmospheres*, 118, 11,175–11,186,
841 <https://doi.org/10.1002/jgrd.50856>, 2013.

842 Kravitz, B., Wang, H., Rasch, P. J., Morrison, H., and Solomon, A. B.: Process-model simulations of cloud albedo
843 enhancement by aerosols in the Arctic, *Phil. Trans. R. Soc. A.*, 372, 20140052, <https://doi.org/10.1098/rsta.2014.0052>,
844 2014.

845 Latham, J., Rasch, P., Chen, C.-C., Kettles, L., Gadian, A., Gettelman, A., Morrison, H., Bower, K., and Choulaton, T.:
846 Global temperature stabilization via controlled albedo enhancement of low-level maritime clouds, *Philosophical*
847 *Transactions of the Royal Society A: Mathematical, Physical and Engineering Sciences*, 366, 3969–3987,
848 <https://doi.org/10.1098/rsta.2008.0137>, 2008.

849 Latham, J., Bower, K., Choulaton, T., Coe, H., Connolly, P., Cooper, G., Craft, T., Foster, J., Gadian, A., Galbraith, L.,
850 Iacovides, H., Johnston, D., Launder, B., Leslie, B., Meyer, J., Neukermans, A., Ormond, B., Parkes, B., Rasch, P., Rush,
851 J., Salter, S., Stevenson, T., Wang, H., Wang, Q., and Wood, R.: Marine cloud brightening, *Philosophical Transactions*
852 *of the Royal Society A: Mathematical, Physical and Engineering Sciences*, 370, 4217–4262,
853 <https://doi.org/10.1098/rsta.2012.0086>, 2012.

854 Latham, J., Gadian, A., Fournier, J., Parkes, B., Wadhams, P., and Chen, J.: Marine cloud brightening: regional
855 applications, *Philosophical Transactions of the Royal Society A: Mathematical, Physical and Engineering Sciences*, 372,
856 20140053, <https://doi.org/10.1098/rsta.2014.0053>, 2014.

857 Lenton, T. M. and Vaughan, N. E.: The radiative forcing potential of different climate geoengineering options,
858 *Atmospheric Chemistry and Physics*, 9, 5539–5561, <https://doi.org/10.5194/acp-9-5539-2009>, 2009.

859 Liu, F., Mao, F., Rosenfeld, D., Pan, Z., Zang, L., Zhu, Y., Yin, J., and Gong, W.: Opposing comparable large effects of
860 fine aerosols and coarse sea spray on marine warm clouds, *Commun Earth Environ*, 3, 1–9,
861 <https://doi.org/10.1038/s43247-022-00562-y>, 2022.

862 Liu, Z., Wang, M., Rosenfeld, D., Zhu, Y., Bai, H., Cao, Y., and Liang, Y.: Evaluation of Cloud and Precipitation
863 Response to Aerosols in WRF-Chem With Satellite Observations, *Journal of Geophysical Research: Atmospheres*, 125,
864 e2020JD033108, <https://doi.org/10.1029/2020JD033108>, 2020.

865 Mahfouz, N. G. A., Hill, S. A., Guo, H., and Ming, Y.: The Radiative and Cloud Responses to Sea Salt Aerosol
866 Engineering in GFDL Models, *Geophysical Research Letters*, 50, e2022GL102340,
867 <https://doi.org/10.1029/2022GL102340>, 2023.

868 Mengel, M., Nauels, A., Rogelj, J., and Schleussner, C.-F.: Committed sea-level rise under the Paris Agreement and the
869 legacy of delayed mitigation action, *Nat Commun*, 9, 601, <https://doi.org/10.1038/s41467-018-02985-8>, 2018.

870 Monahan, E. C., Spiel, D. E., and Davidson, K. L.: A Model of Marine Aerosol Generation Via Whitecaps and Wave
871 Disruption, in: *Oceanic Whitecaps: And Their Role in Air-Sea Exchange Processes*, edited by: Monahan, E. C. and
872 Niocaill, G. M., Springer Netherlands, Dordrecht, 167–174, https://doi.org/10.1007/978-94-009-4668-2_16, 1986.

873 Morrison, H., Thompson, G., and Tatarskii, V.: Impact of Cloud Microphysics on the Development of Trailing Stratiform
874 Precipitation in a Simulated Squall Line: Comparison of One- and Two-Moment Schemes, *Monthly Weather Review*,
875 137, 991–1007, <https://doi.org/10.1175/2008mwr2556.1>, 2009.

876 Niemeier, U., Schmidt, H., Alterskjær, K., and Kristjánsson, J. E.: Solar irradiance reduction via climate engineering:
877 Impact of different techniques on the energy balance and the hydrological cycle, *Journal of Geophysical Research:*
878 *Atmospheres*, 118, 11,905-11,917, <https://doi.org/10.1002/2013JD020445>, 2013.

879 Partanen, A.-I., Kokkola, H., Romakkaniemi, S., Kerminen, V.-M., Lehtinen, K. E. J., Bergman, T., Arola, A., and
880 Korhonen, H.: Direct and indirect effects of sea spray geoengineering and the role of injected particle size, *Journal of*
881 *Geophysical Research: Atmospheres*, 117, <https://doi.org/10.1029/2011JD016428>, 2012.

882 Paulot, F., Paynter, D., Winton, M., Ginoux, P., Zhao, M., and Horowitz, L. W.: Revisiting the Impact of Sea Salt on
883 Climate Sensitivity, *Geophysical Research Letters*, 47, e2019GL085601, <https://doi.org/10.1029/2019GL085601>, 2020.

884 Pleim, J. E.: A Combined Local and Nonlocal Closure Model for the Atmospheric Boundary Layer. Part I: Model
885 Description and Testing, *Journal of Applied Meteorology and Climatology*, 46, 1383–1395,

886 <https://doi.org/10.1175/jam2539.1>, 2007.

887 Pringle, K. J., Carslaw, K. S., Fan, T., Mann, G. W., Hill, A., Stier, P., Zhang, K., and Tost, H.: A multi-model assessment
888 of the impact of sea spray geoengineering on cloud droplet number, *Atmospheric Chemistry and Physics*, 12, 11647–
889 11663, <https://doi.org/10.5194/acp-12-11647-2012>, 2012.

890 Quaas, J., Boucher, O., Bellouin, N., and Kinne, S.: Satellite-based estimate of the direct and indirect aerosol climate
891 forcing, *Journal of Geophysical Research: Atmospheres*, 113, <https://doi.org/10.1029/2007JD008962>, 2008.

892 ~~Ramaswamy, V., Boucher, O., Haigh, J., Hauglustaine, D., Haywood, J., Myhre, G., Nakajima, T., Shi, G. Y., Solomon,
893 S., Betts, R., Charlson, R., Chuang, C., Daniel, J. S., Joos, F., and Srinivasan, J.: Radiative Forcing of Climate Change,
894 2001.~~

895 ~~Rasch, P., Hirasawa, H., Wu, M., Doherty, S., Wood, R., Wang, H., Jones, A., Haywood, J., and Singh, H.: A protocol for
896 model intercomparison of impacts of Marine Cloud Brightening Climate Intervention, *EGUsphere*, 1–43,
897 <https://doi.org/10.5194/egusphere-2024-1031>, 2024.~~

898 Rasch, P. J., Latham, J., and Chen, C.-C. (Jack): Geoengineering by cloud seeding: influence on sea ice and climate
899 system, *Environ. Res. Lett.*, 4, 045112, <https://doi.org/10.1088/1748-9326/4/4/045112>, 2009.

900 Rosenfeld, Daniel, Sherwood, Steven, Wood, Robert, Donner, and Leo: Climate Effects of Aerosol-Cloud Interactions.,
901 *Science*, <https://doi.org/10.1126/science.1247490>, 2014.

902 Rosenfeld, D., Zhu, Y., Wang, M., Zheng, Y., Goren, T., and Yu, S.: Aerosol-driven droplet concentrations dominate
903 coverage and water of oceanic low-level clouds, *Science*, 363, eaav0566, <https://doi.org/10.1126/science.aav0566>, 2019.

904 Salter, S., Sortino, G., and Latham, J.: Sea-going hardware for the cloud albedo method of reversing global warming,
905 *Philosophical Transactions of the Royal Society A: Mathematical, Physical and Engineering Sciences*, 366, 3989–4006,
906 <https://doi.org/10.1098/rsta.2008.0136>, 2008.

907 Stjern, C. W., Muri, H., Ahlm, L., Boucher, O., Cole, J. N. S., Ji, D., Jones, A., Haywood, J., Kravitz, B., Lenton, A.,
908 Moore, J. C., Niemeier, U., Phipps, S. J., Schmidt, H., Watanabe, S., and Kristjánsson, J. E.: Response to marine cloud
909 brightening in a multi-model ensemble, *Atmospheric Chemistry and Physics*, 18, 621–634, <https://doi.org/10.5194/acp-18-621-2018>, 2018.

911 Stuart, G. S., Stevens, R. G., Partanen, A.-I., Jenkins, A. K. L., Korhonen, H., Forster, P. M., Spracklen, D. V., and Pierce,
912 J. R.: Reduced efficacy of marine cloud brightening geoengineering due to in-plume aerosol coagulation:
913 parameterization and global implications, *Atmospheric Chemistry and Physics*, 13, 10385–10396,
914 <https://doi.org/10.5194/acp-13-10385-2013>, 2013.

915 Twomey, S.: Pollution and the planetary albedo, *Atmospheric Environment* (1967), 8, 1251–1256,
916 [https://doi.org/10.1016/0004-6981\(74\)90004-3](https://doi.org/10.1016/0004-6981(74)90004-3), 1974.

917 Visioni, D., Kravitz, B., Robock, A., Tilmes, S., Haywood, J., Boucher, O., Lawrence, M., Irvine, P., Niemeier, U., Xia,
918 L., Chiodo, G., Lennard, C., Watanabe, S., Moore, J. C., and Muri, H.: Opinion: The scientific and community-building
919 roles of the Geoengineering Model Intercomparison Project (GeoMIP) – past, present, and future, *Atmospheric
920 Chemistry and Physics*, 23, 5149–5176, <https://doi.org/10.5194/acp-23-5149-2023>, 2023.

921 Wang, K., Zhang, Y., Yu, S., Wong, D. C., Pleim, J., Mathur, R., Kelly, J. T., and Bell, M.: A comparative study of two-
922 way and offline coupled WRF v3.4 and CMAQ v5.0.2 over the contiguous US: performance evaluation and impacts of

923 chemistry–meteorology feedbacks on air quality, *Geoscientific Model Development*, 14, 7189–7221,
924 <https://doi.org/10.5194/gmd-14-7189-2021>, 2021.

925 Wong, D. C., Pleim, J., Mathur, R., Binkowski, F., Otte, T., Gilliam, R., Pouliot, G., Xiu, A., Young, J. O., and Kang, D.:
926 WRF-CMAQ two-way coupled system with aerosol feedback: software development and preliminary results,
927 *Geoscientific Model Development*, 5, 299–312, <https://doi.org/10.5194/gmd-5-299-2012>, 2012.

928 Wood, R.: Assessing the potential efficacy of marine cloud brightening for cooling Earth using a simple heuristic model,
929 *Atmospheric Chemistry and Physics*, 21, 14507–14533, <https://doi.org/10.5194/acp-21-14507-2021>, 2021.

930 Yu, S., Mathur, R., Pleim, J., Wong, D., Gilliam, R., Alapaty, K., Zhao, C., and Liu, X.: Aerosol indirect effect on the
931 grid-scale clouds in the two-way coupled WRF–CMAQ: model description, development, evaluation and regional
932 analysis, *Atmospheric Chemistry and Physics*, 14, 11247–11285, <https://doi.org/10.5194/acp-14-11247-2014>, 2014.

933 Zhang, K. M., Knipping, E. M., Wexler, A. S., Bhave, P. V., and Tonnesen, G. S.: Size distribution of sea-salt emissions
934 as a function of relative humidity, *Atmospheric Environment*, 39, 3373–3379,
935 <https://doi.org/10.1016/j.atmosenv.2005.02.032>, 2005.

936 Zhao, D., Lin, Y., Dong, W., Qin, Y., Chu, W., Yang, K., Letu, H., and Huang, L.: Alleviated WRF Summer Wet Bias
937 Over the Tibetan Plateau Using a New Cloud Microphysics Scheme, *Journal of Advances in Modeling Earth Systems*,
938 15, e2023MS003616, <https://doi.org/10.1029/2023MS003616>, 2023.

939 ~~Zhao, G., Zhao, C., Kuang, Y., Bian, Y., Tao, J., Shen, C., and Yu, Y.: Calculating the aerosol asymmetry factor based on
940 measurements from the humidified nephelometer system, *Atmospheric Chemistry and Physics*, 18, 9049–9060,
941 <https://doi.org/10.5194/acp-18-9049-2018>, 2018.~~ Cao, L., Duan, L., Bala, G., and Caldeira, K.: Climate More
942 Responsive to Marine Cloud Brightening Than Ocean Albedo Modification: A Model Study, *Journal of Geophysical
943 Research: Atmospheres*, 126, e2020JD033256, <https://doi.org/10.1029/2020JD033256>, 2021.

944 ~~Zhao, M., Cao, L., Duan, L., Bala, G., and Caldeira, K.: Climate More Responsive to Marine Cloud Brightening Than
945 Ocean Albedo Modification: A Model Study, *Journal of Geophysical Research: Atmospheres*, 126, e2020JD033256,
946 <https://doi.org/10.1029/2020JD033256>, 2021.~~

947

Table 1. The cloud fraction, CDNC, LWP, and regional sea-salt aerosol concentrations at Base and after injection of sea-salt aerosols at $10^{-9} \text{ kg m}^{-2} \text{ s}^{-1}$ (Exp) for five ocean regions.

Areas	Cloud Fraction		CDNC (# cm ⁻³)		LWP (g m ⁻²)		Regional sea-salt aerosols (μg m ⁻³)	
	Base	Exp	Base	Exp	Base	Exp	Base	Exp
WP	0.0445	0.0488	19.3	100	12.8	19.8	8.91	143
NP	0.0678	0.0760	9.67	60.2	24.6	43.9	7.18	126
Equa	0.0051	0.0059	17.5	83.4	0.85	1.39	7.32	102
SP	0.0547	0.0617	11.5	89.4	21.6	38.9	6.79	176
SA	0.0519	0.0575	12.3	92.2	23.5	41.6	7.00	149

Table 2. Differences (Exp - Base) in SW_TOT, SW_CLD, SW_AER and SW_AER_CLR at the TOA due to the injection of sea-salt aerosols in different strategies in five ocean regions.

Strategies	Areas	SW_TOT (W m ⁻²)	SW_CLD (W m ⁻²)	SW_AER (W m ⁻²)	SW_AER_CLR (W m ⁻²)
Natural×5	AsiaWP	0.6046	0.4935	0.11	0.16
	NP	2.081	1.962.0	0.11	0.19
	Equa	0.0607	-0.01	0.0706	0.07
	SP	1.557	1.4659	0.08	0.14
	SA	1.434	1.3226	0.11	0.16
Wind-adjusted	AsiaWP	4.023.8	2.091.9	1.939	2.303
	NP	8.474	6.898	1.596	2.354
	Equa	1.354	0.1727	1.182	1.212
	SP	7.756	5.948	1.818	2.576
	SA	7.918.0	5.869	2.051	2.838
10 ⁻⁹ kg m ⁻² s ⁻¹	AsiaWP	17.3418	4.406	12.9413	15.35
	NP	23.11	13.41	9.708	14.5115
	Equa	10.9611	0.5455	10.42	10.6811
	SP	24.5025	10.7311	13.7714	18.6719
	SA	22.36	11.27	11.08	15.33
10 ⁻⁹ kg m ⁻² s ⁻¹ in the sensitive area	Asia	0.65	0.16	0.49	0.60
	NP	2.69	2.01	0.68	0.97
	Equa	0.74	0.10	0.64	0.65
	SP	3.27	2.24	1.04	1.35
	SA	1.81	1.20	0.61	0.79
Fixed-wind- adjusted	AsiaWP	7.216.9	3.212.9	3.994.0	5.141
	NP	16.07	11.07	5.001	7.738
	Equa	5.000	0.4850	4.535	4.727
	SP	16.4017	9.819	6.596	9.768
	SA	19.7820	10.7911	8.989.1	12.5413

设置了格式: 字体: Times New Roman, 字体颜色: 自动设置

设置了格式: 字体: (默认) 宋体, 字体颜色: 红色
带格式的: 制表位: 不在 19.66 字符

Note: SW_TOT is upward shortwave radiative flux at the TOA for all-sky conditions. The response of SW_TOT to the sea-salt aerosols injection can be separated into the influence of the cloud radiative effect (SW_CLD, where the influence of the aerosol is excluded) and the influence of the aerosol direct scattering effect (SW_AER) in the presence of clouds. That is, $SW_TOT = SW_CLD + SW_AER$. The SW_AER_CLR is the response of aerosol direct scattering to the upward shortwave radiative flux at the TOA under clear skies.

Areas	CRF' _{param}			$\frac{\Delta\alpha}{\Delta \ln \text{AOD}}$		
	$\alpha'_c \bar{f}$	$\bar{\alpha}_c f'$	$\alpha'_c f'$	Twomey Effect	LWP Effect	Cloud Fraction Effect
WP	71.5%	20.7%	7.82%	48.4%	41.6%	10.1%
NP	72.7%	16.9%	10.4%	48.5%	41.7%	9.71%
Equa	60.2%	27.3%	12.4%	36.4%	58.5%	5.09%
SP	73.8%	15.9%	10.3%	51.8%	39.0%	9.19%
SA	77.3%	13.9%	8.81%	52.5%	39.7%	7.78%

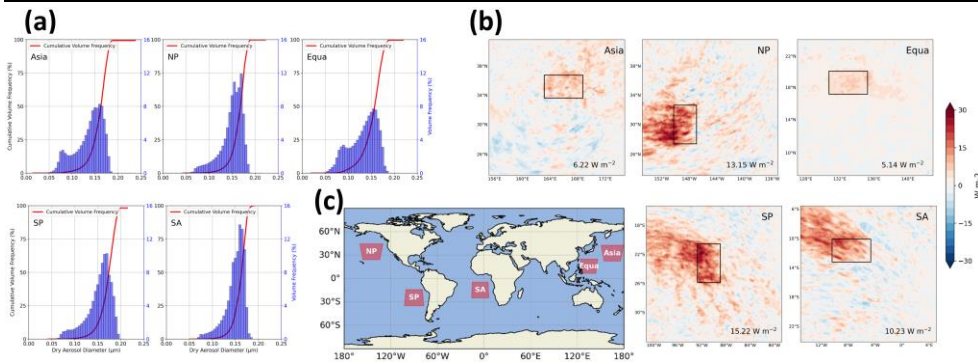


Table 3. Relative effects of cloud fraction and albedo changes on CRF'_{param} and Twomey, LWP, and cloud fraction effects to SW CLD responses after uniform fixed injection of $10^{-9} \text{ kg m}^{-2} \text{ s}^{-1}$ sea-salt aerosols over five ocean regions.

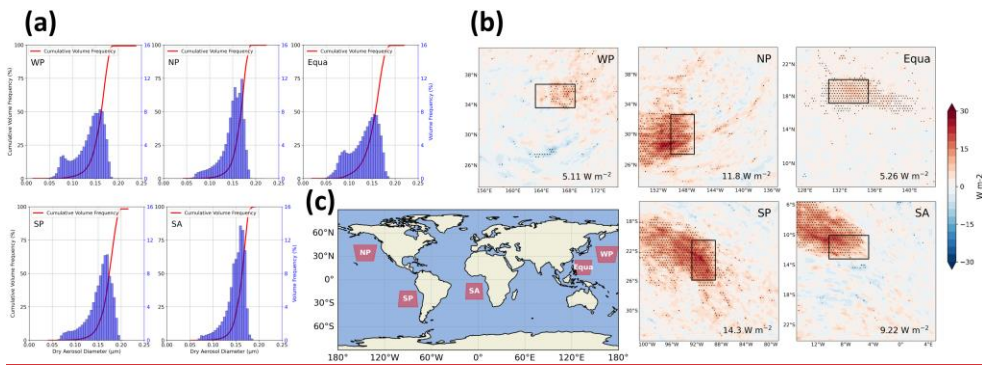


Figure 1. Injecting sea-salt aerosols into five open sea regions to simulate the implementation of MCB geoengineering. **(a)** The cumulative volume frequency of increased aerosol dry particle size- (uniform injection of $10^{-9} \text{ kg m}^{-2} \text{ s}^{-1}$ sea-salt aerosols over the entire region). **(b)** Differences (Exp - Base) in the spatial distribution of the TOA upward shortwave radiative flux response (SW_TOT) resulting from uniform injection of $10^{-9} \text{ kg m}^{-2} \text{ s}^{-1}$ sea-salt aerosol in sensitive areas in five ocean regions, with SW_TOT response values resulting only in sensitive areas labeled in the lower right corner. Areas labeled with dots indicate mean differences that are significant at the 95% confidence level. Black rectangles are sensitive areas. **(c)** Location of the five ocean modeling domains.

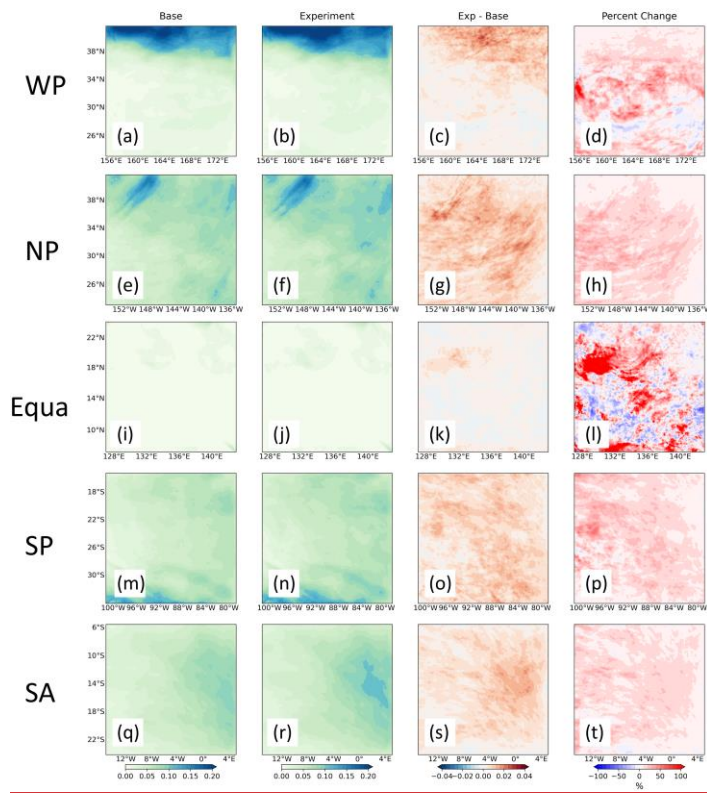
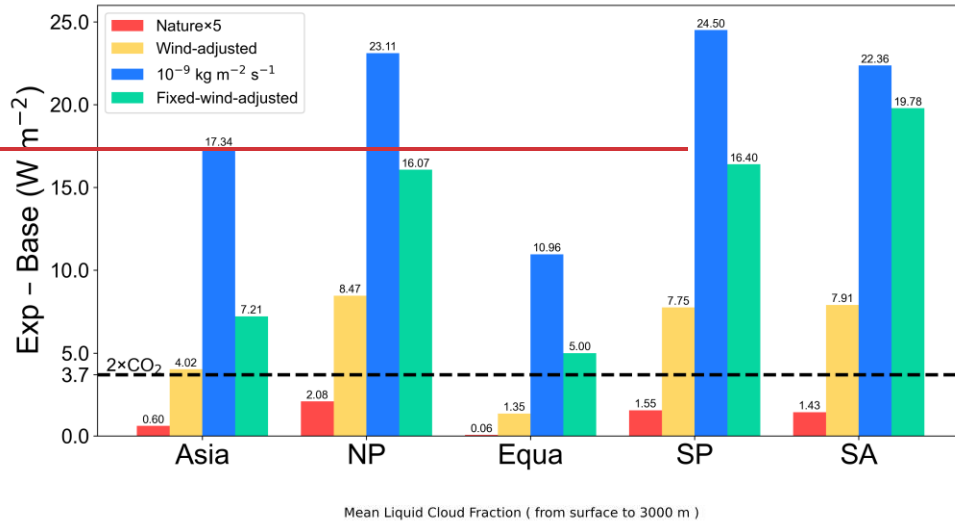


Figure 2. Differences in SW_TOT due to Column mean liquid cloud fraction from the surface to 3000 m

altitude for five regions. The first to fourth columns are Base, the sensitivity experiment with a uniform injection of $10^{-9} \text{ kg m}^{-2} \text{ s}^{-1}$ sea-salt aerosols in different ways in five ocean regions. The black dashed line is the radiative flux response required to offset over the 3.7 W m^{-2} radiative forcing caused by entire region, Exp - Base, and the doubling percent change of atmospheric CO_2 concentrations since industrialization Exp - Base, respectively.

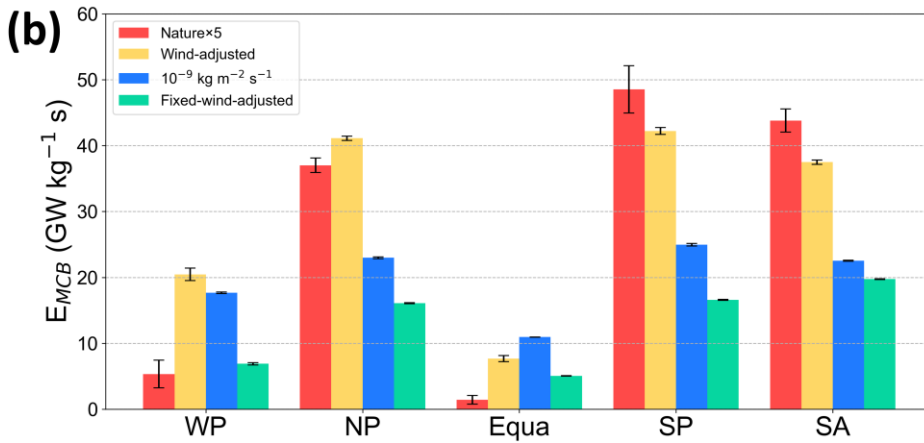
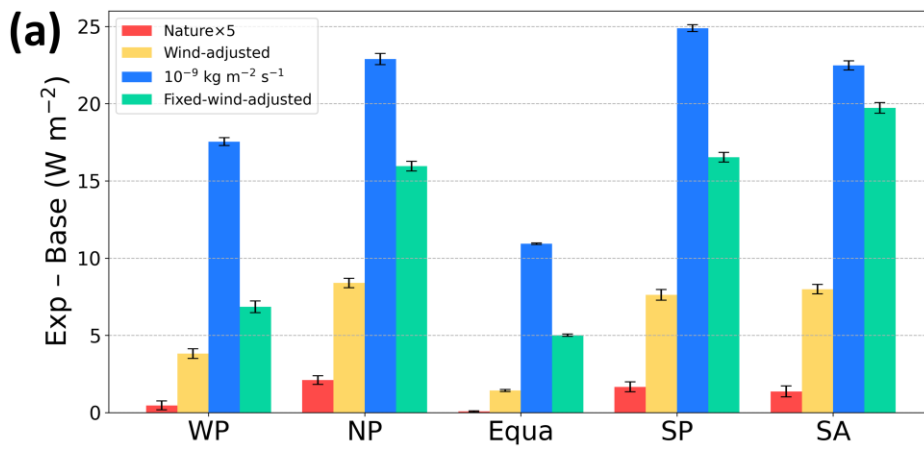
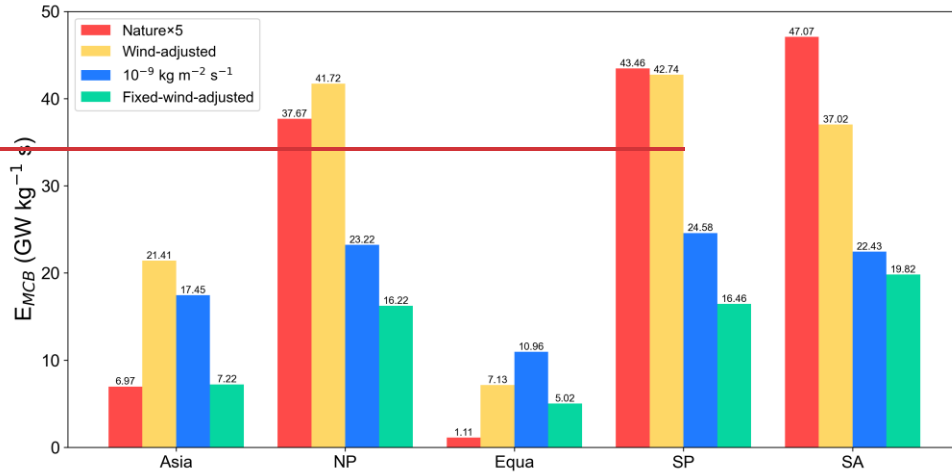
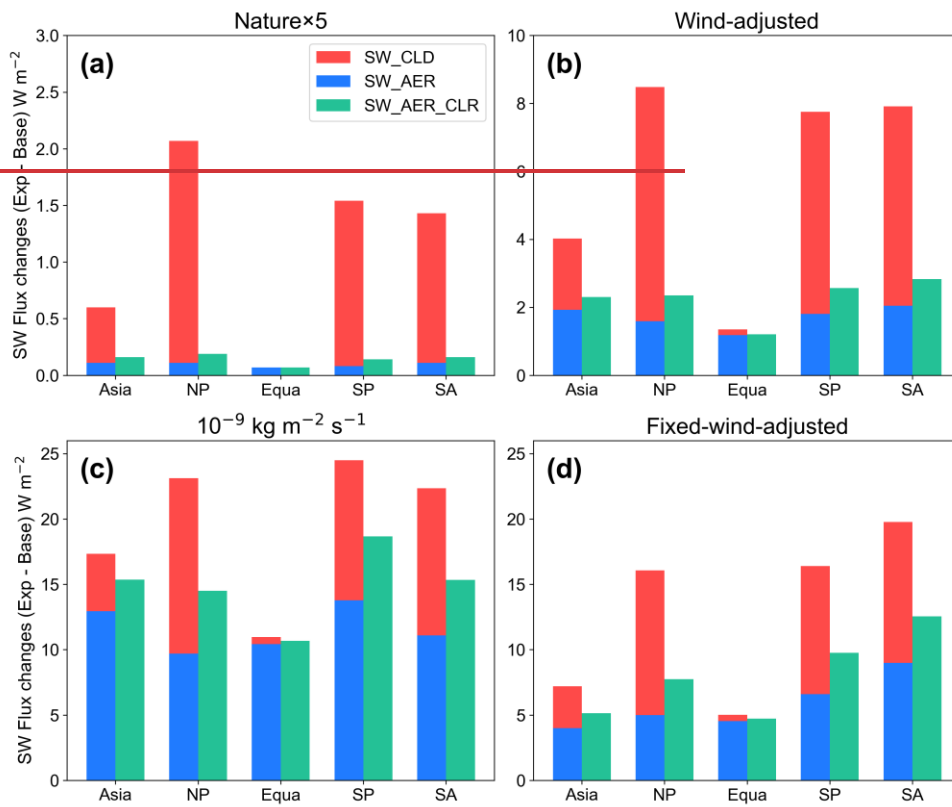


Figure 3. (a) The differences in SW_{TOT} and (b) the MCB efficiency (E_{MCB}) after due to the injection of sea-salt aerosols in different strategies in five sea areas/ocean regions.

带格式的: 两端对齐

设置了格式: 字体: 非加粗



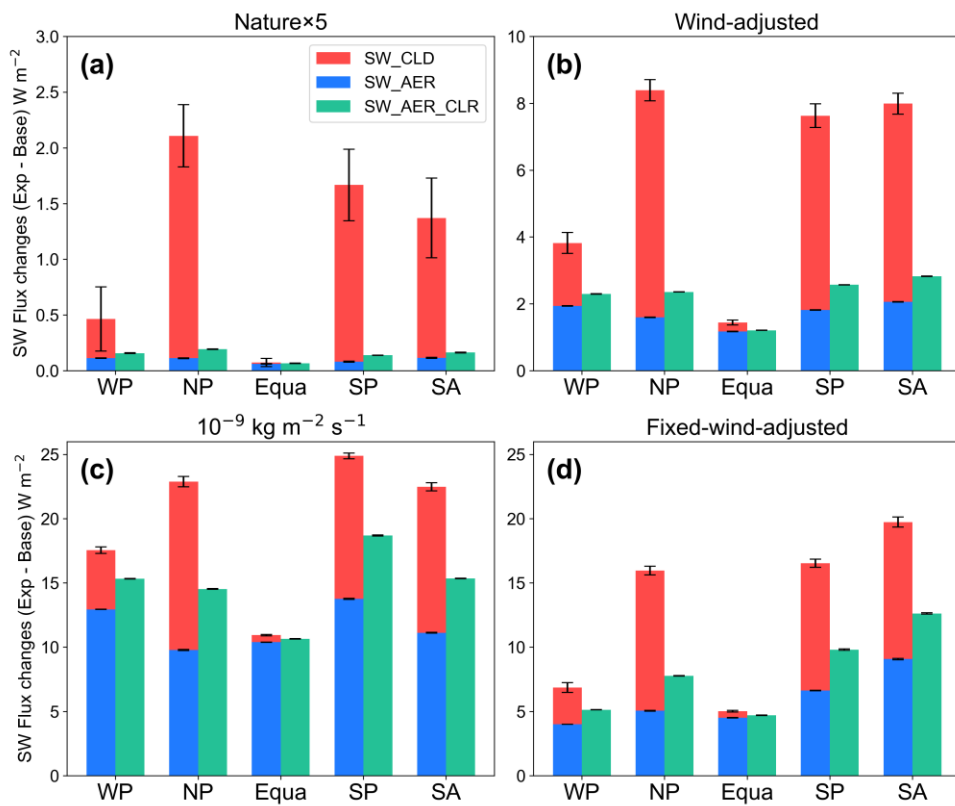
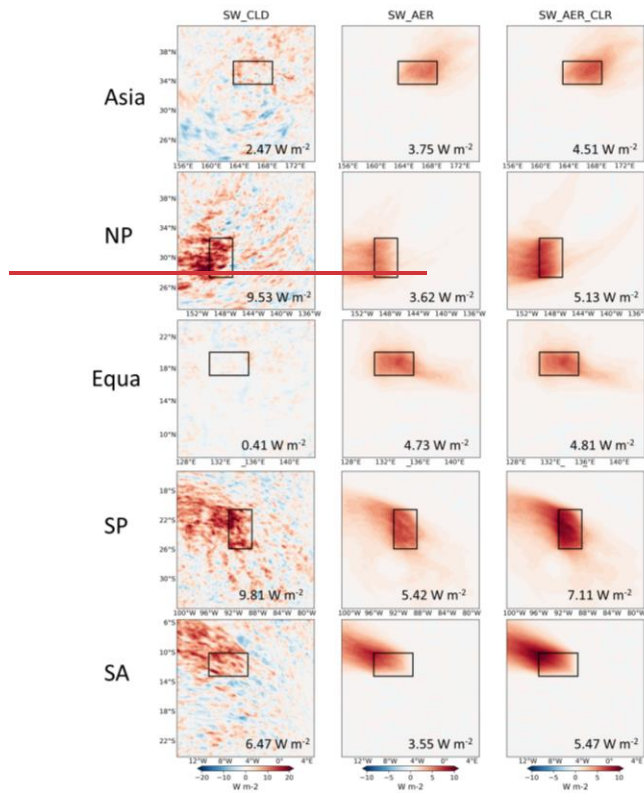


Figure 4. Decomposition of the upward shortwave radiative fluxes at the TOA due to the different ways/strategies of injecting sea-salt aerosols in the five regions. Note that the vertical coordinate y-axis ranges are not consistent.



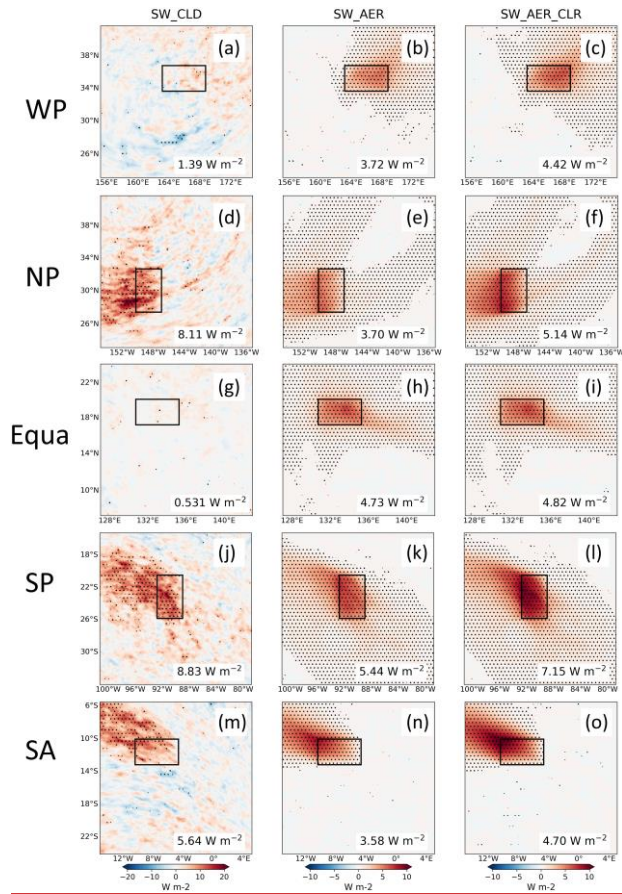


Figure 5. Spatial distribution of SW_CLD (first column), SW_AER (second column), and SW_AER_CLR (third column) responses resulting from the injection of $10^{-9} \text{ kg m}^{-2} \text{ s}^{-1}$ sea-salt aerosols in the sensitive areas over five ocean regions. The values of the radiative flux responses generated only in the sensitive area are labeled in the lower right corner. Areas labeled with dots indicate mean differences that are significant at the 95% confidence level. The black rectangles are sensitive areas.

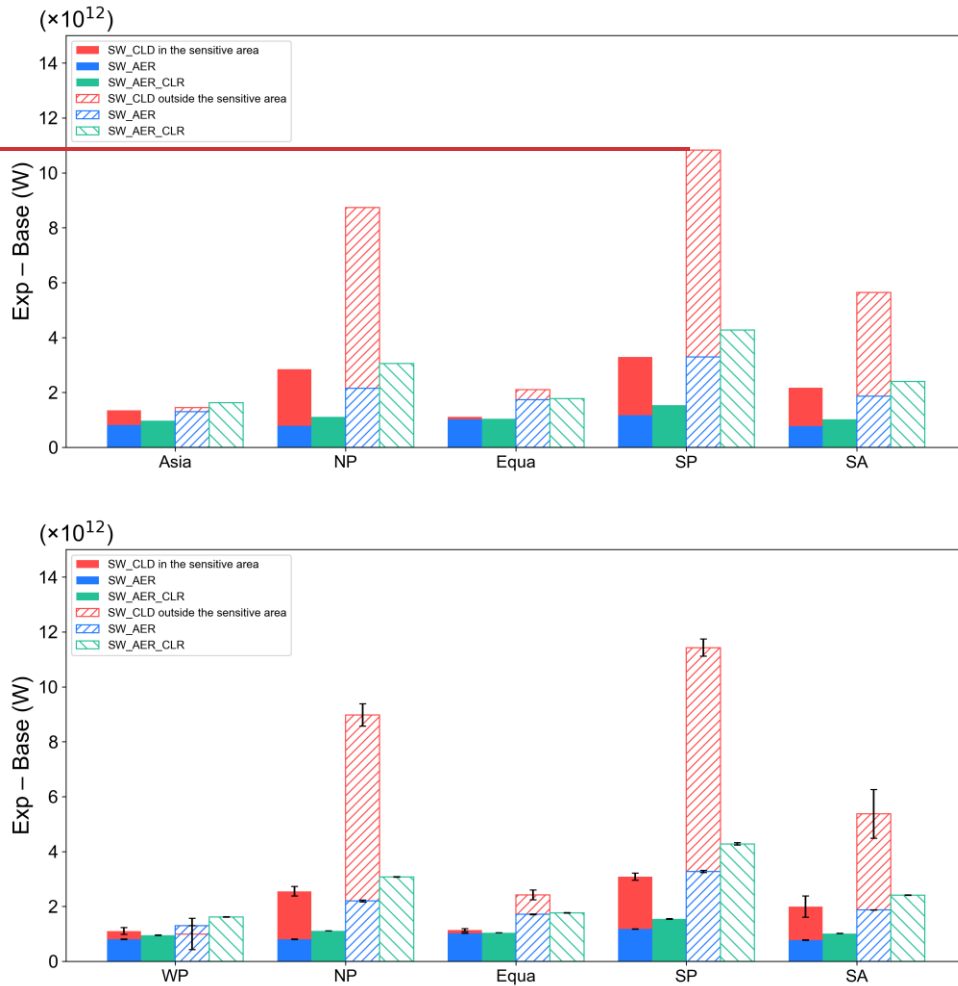
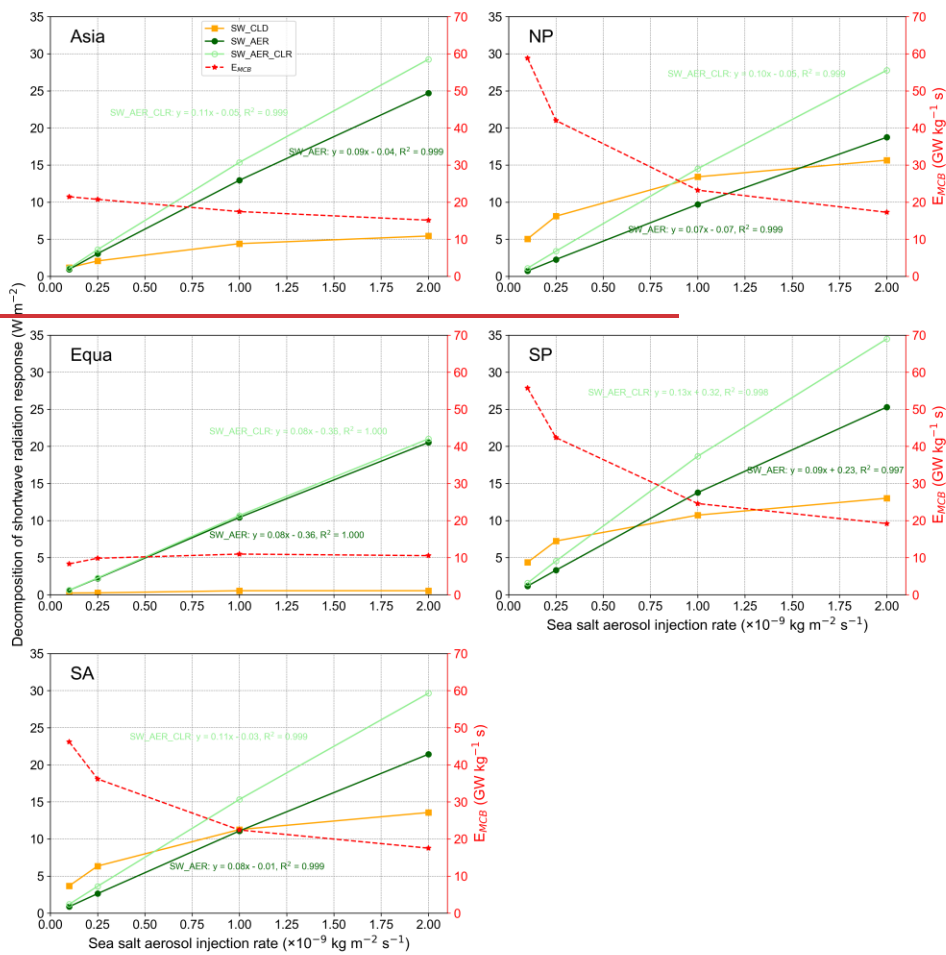


Figure 6. Total SW_CLD, SW_AER, and SW_AER_CLR responses resulting from the injection of 10^{-9} $\text{kg m}^{-2} \text{s}^{-1}$ sea-salt aerosols within the sensitive areas of the five regions. The solid columns indicate the total radiative response calculated for aerosol injection within the sensitive areas. Columns filled with ~~hatching~~ indicate the total radiative response outside the sensitive areas.



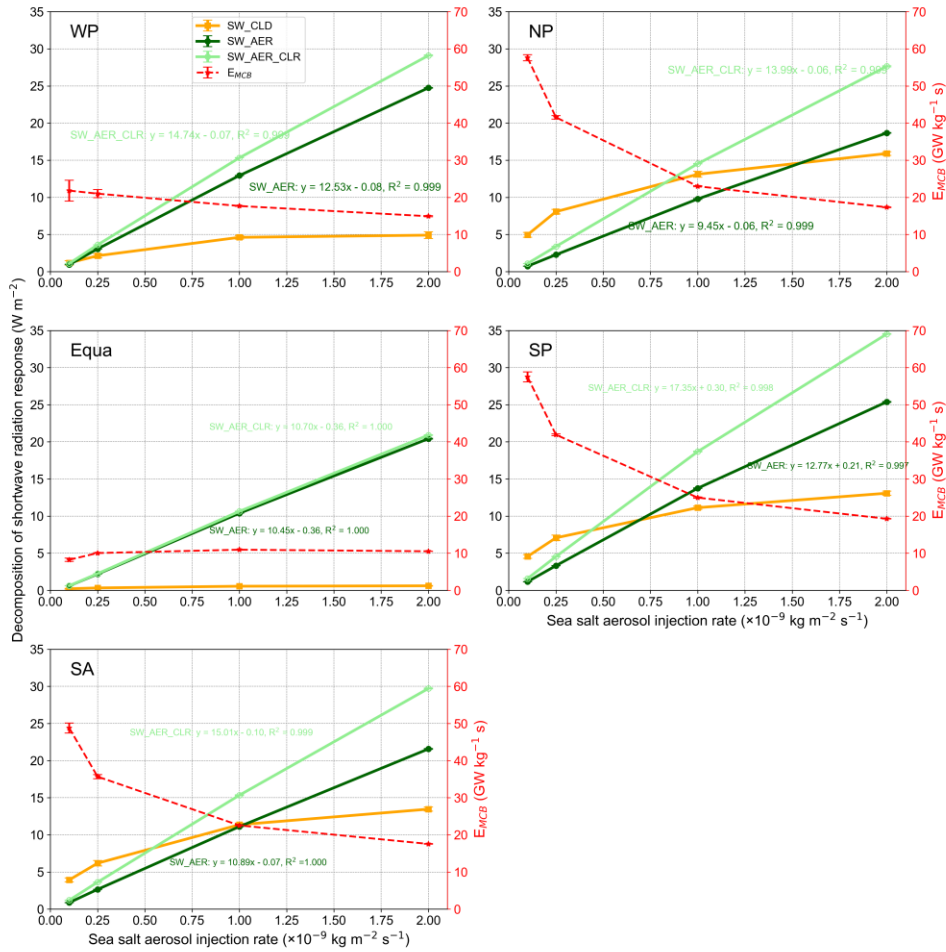
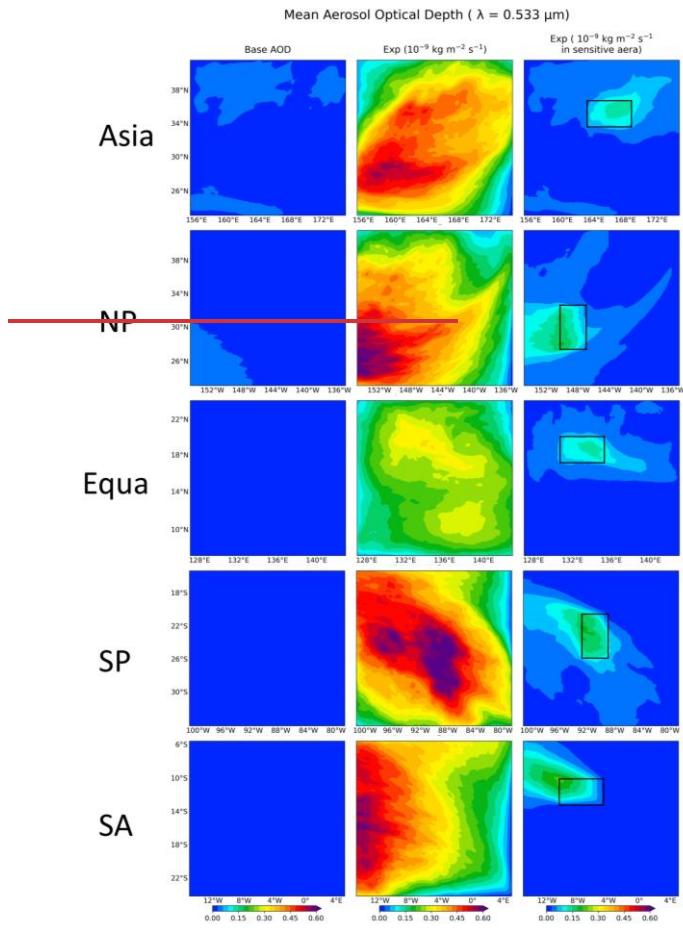


Figure 7. Changes in SW_CLD, SW_AER, and SW_AER_CLR radiative responses due to sea-salt aerosols uniformly injected in varying amounts in five ocean regions, and corresponding changes in E_{MCB} . SW_AER and SW_AER_CLR are labeled with the results of the corresponding linear regression analysis.



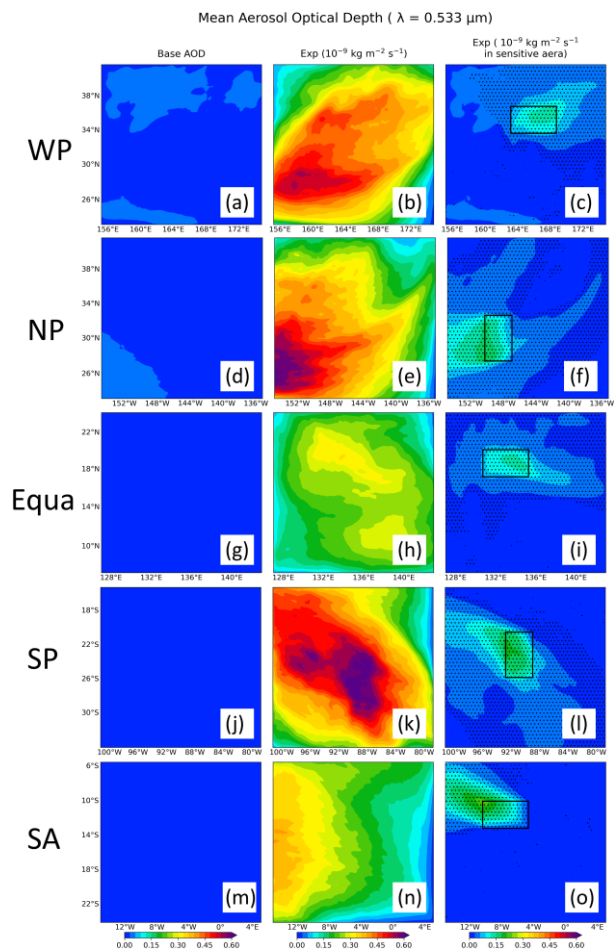


Figure 8. Spatial distribution of mean AOD ($\lambda = 0.533 \mu\text{m}$) for five ocean regions. The first column is the AOD for Base, the second column is the AOD after uniform injection at $10^{-9} \text{ kg m}^{-2} \text{ s}^{-1}$, and the third column is the AOD after uniform injection in sensitive areas. Areas labeled with dots indicate mean differences that are significant at the 95% confidence level. The black rectangles are sensitive areas.

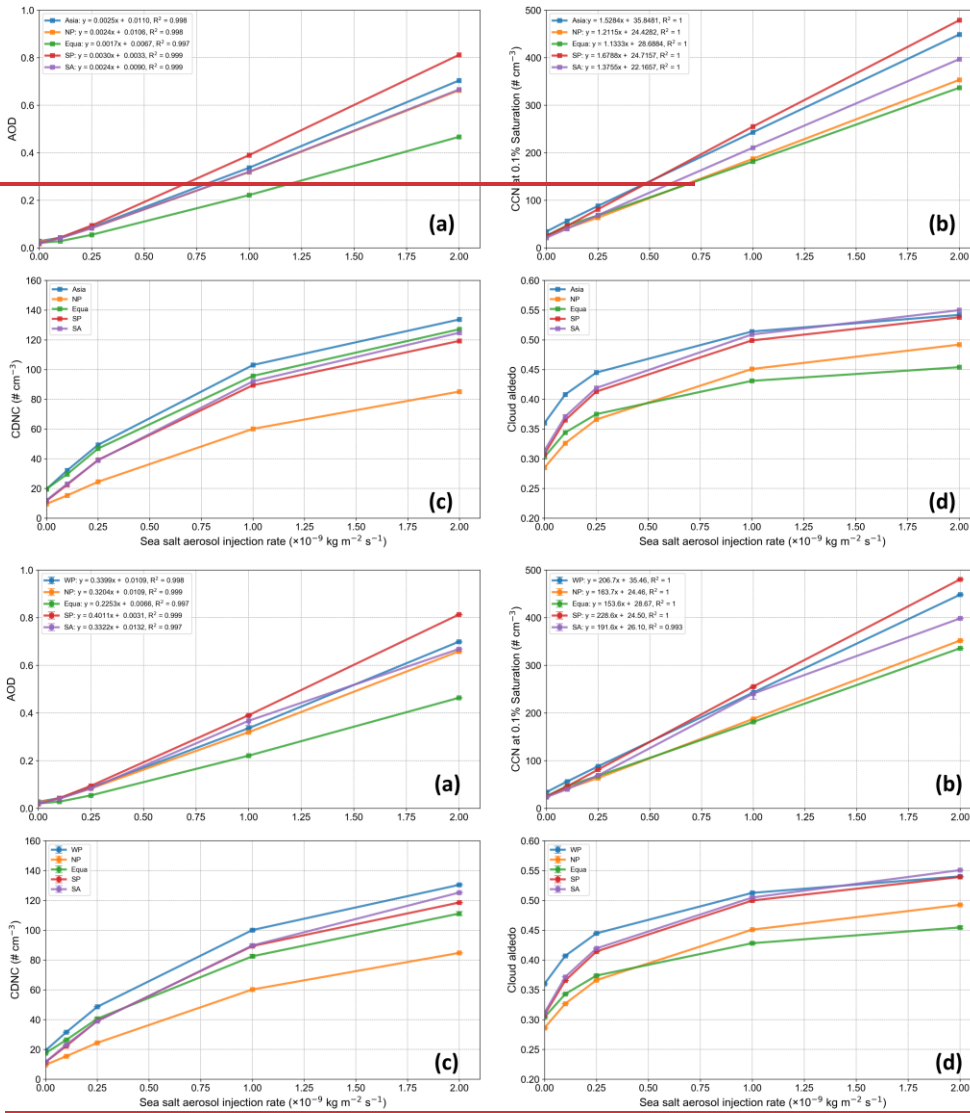
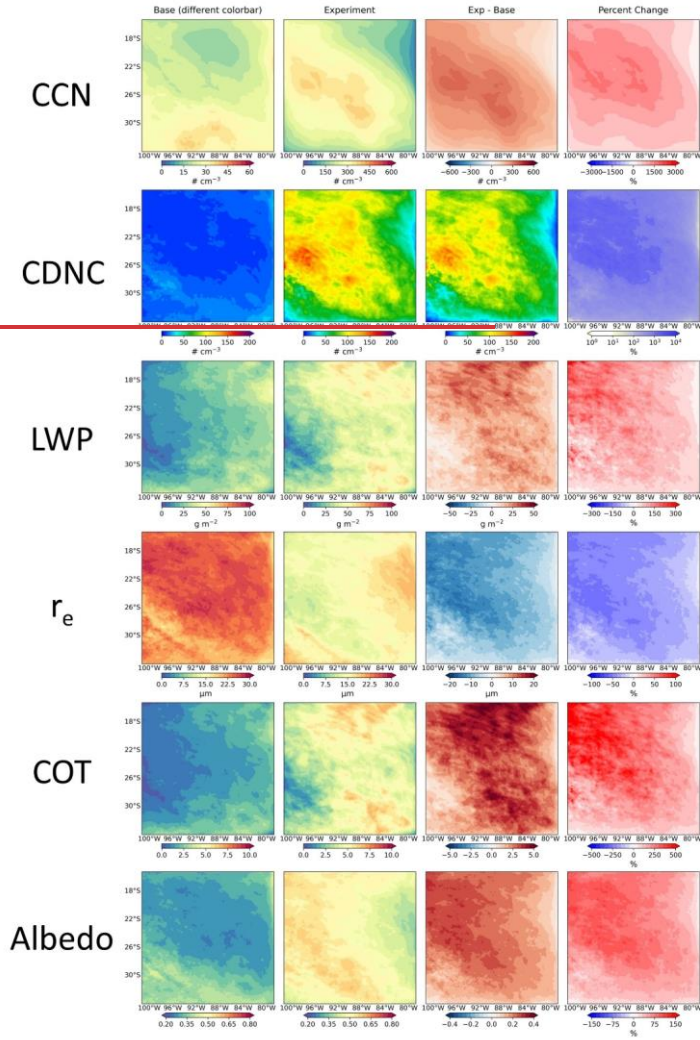


Figure 9. Relationship between changes in regional mean (a) AOD, (b) CCN, (c) CDNC, and (d) cloud albedo due to uniform injection of sea-salt aerosols across the region and the amounts of sea-salt aerosols injected. The results of the linear regression of (a) AOD and (b) CCN on the sea-salt aerosols injection amount are given at the legends.

For SP ($10^{-9} \text{ kg m}^{-2} \text{ s}^{-1}$ injection)



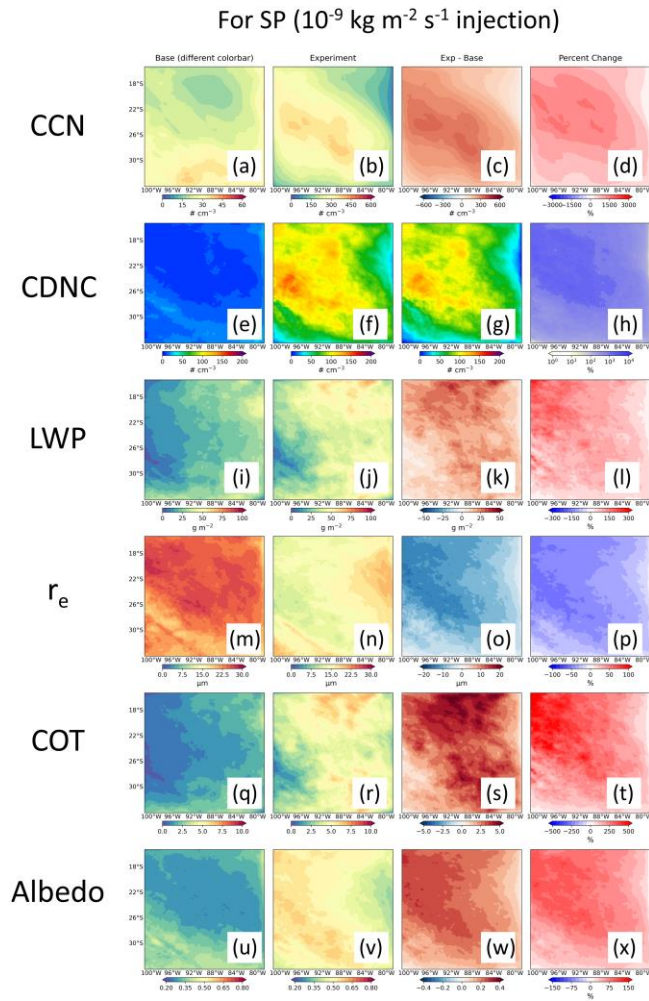
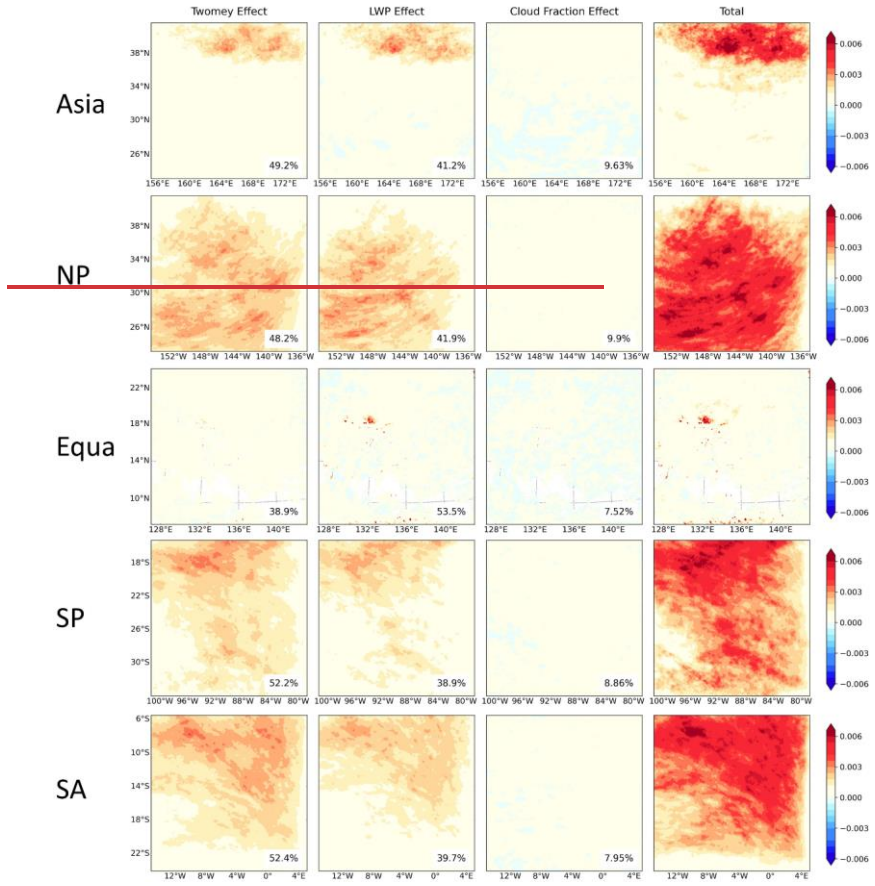


Figure 10. Spatial distribution of liquid cloud property responses after uniform injection of sea-salt aerosols with $10^{-9} \text{ kg m}^{-2} \text{ s}^{-1}$ in the SP region. Results are shown for cloud condensation nuclei (CCN, $S = 0.1\%$, $\# \text{ cm}^{-3}$), cloud droplet number concentration ($\# \text{ cm}^{-3}$), liquid water path (LWP, g m^{-2}), cloud effective radius (r_e , μm), cloud optical thickness (COT), and cloud albedo for Base (first column), Exp (second column), Exp - Base (third column), and the percentage change in Exp - Base (fourth column), respectively.

Mean Total Aerosol Radiative Forcing Components - Twomey, LWP, CLDFRA



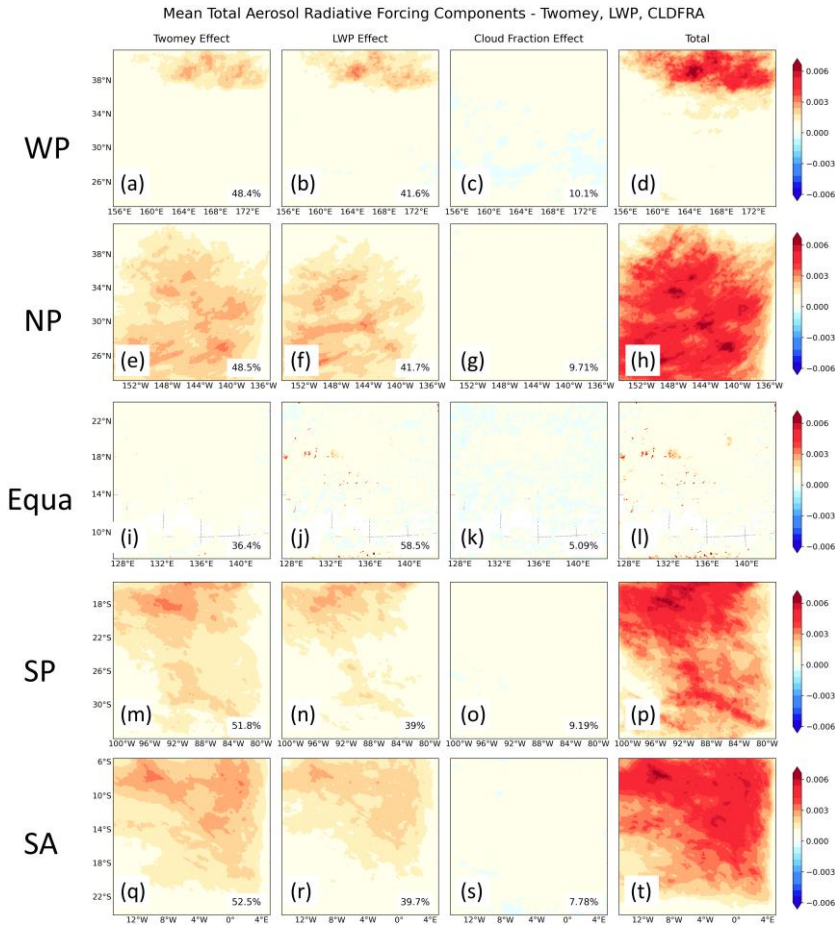


Figure 11. Spatial distribution of cloud property changes in response to SW_CLD radiation after uniform injection of sea-salt aerosols in five regions. The first column is the Twomey effect, the second column is the LWP effect, the third column is the cloud fraction effect, and the fourth column is the cloud susceptibility ($\frac{\Delta\alpha}{\Delta \ln AOD}$) to aerosol injection for the sum of the three effects. The percentage contribution of each to the total SW_CLD response over the entire region is labeled in the lower right corner.